Miller, L. E., Montroni, L., Koun, E., Salemme, R., Hayward, V., Farnè, A. 2018. **Sensing With Tools Extends Somatosensory Processing Beyond The Body.** *Nature*, 561(7722):239-242.

Sensing with tools extends somatosensory processing beyond the body

Luke E. Miller[1,2,3], Luca Montroni[1,2], Eric Koun[1,2], Romeo Salemme[1,2,3], Vincent Hayward[4,5], Alessandro Farnè[1,2,3,6]

1. Integrative Multisensory Perception Action & Cognition Team - ImpAct, Lyon Neuroscience Research Center, INSERM U1028, CNRS U5292; Lyon, France

2. University of Lyon 1, Lyon, France

3. Hospices Civils de Lyon, Neuro-immersion, Lyon, France

4. Sorbonne Université, UPMC Univ Paris 06, ISIR, F-75005 Paris, France

5. Centre for the Study of the Senses, School of Advanced Study, University of London, London, UK

6. Center for Mind/Brain Sciences, University of Trento, Rovereto, Italy.

* Corresponding authors. Luke E. Miller: luke.miller@inserm.fr; Alessandro Farnè: alessandro.farne@inserm.fr.

The ability to extend sensory information processing beyond the nervous system[1] has been observed throughout the animal kingdom, such as when rodents palpate objects using their whiskers[2] or when spiders localize prey with their webs[3]. We investigated whether the ability to sense objects with tools[4–9] represents an analogous information processing scheme in humans. Rather than mere distal links between the hand and environment[10,11], we propose that tools are treated by the nervous system as sensory extensions of the body. Here we provide evidence from behavioural psychophysics, structural mechanics, and neuronal modelling in support of this claim. We first demonstrate that tool users can accurately sense where an object contacts a wooden rod with surprising accuracy, just as is possible on the skin. We next demonstrate that impact location is encoded by the tool's modal response upon impact, reflecting a pre-neuronal stage of mechanical information processing akin to sensing with whiskers[2] and webs[3]. Lastly, we used a computational model of tactile afferents[12] to demonstrate that impact location can be rapidly re-encoded into a temporally precise spiking code. This code precisely predicts the behavioural of human participants, providing evidence that information encoded in motifs shapes localisation. Thus, we show that this remarkable sensory capability emerges from the functional coupling between material, biomechanical, and neural levels of information processing[13,14].

Historically, researchers across scientific disciplines have focused almost exclusively on motor aspects of tool use[15,16], despite the fact that tools convey behaviourally-relevant sensory information to the user when contacting a surface[17]. Indeed, tactile signals are critical for both hand and tool use since they provide information about objects that is unavailable in other modalities. One familiar example, first discussed in the seventeenth century by René Descartes[18], is a blind person's ability to perceive the environment through the tip of a cane[19] (Fig. 1a). Despite almost four centuries since the publication of Descartes' treatise, scientists have only recently begun investigating how hand-held tools are used to sense properties of the environment, such as object texture[6], position[8], and distance[4]. Tool-mediated sensing is therefore a poorly understood facet of daily human experience.

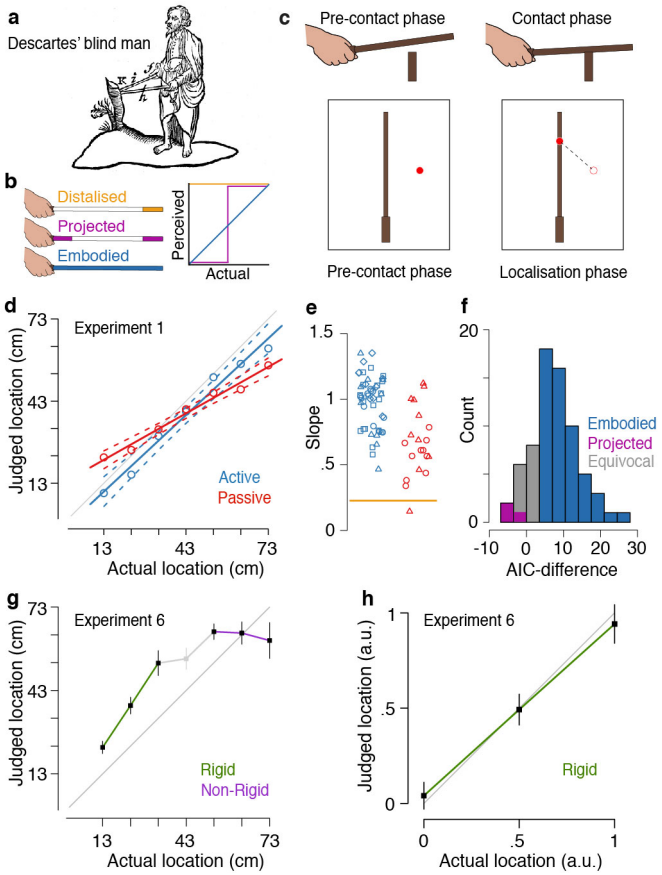

Figure 1. Methods and behavioural results
(a) Descartes' blind man using two canes to triangulate the distance of an object. Image adapted from an illustration made by Descartes. **(b)** Hypothetical models of localisation. Left: Coloured regions correspond to where contact is felt, as predicted by each model. White regions are perceptually "invisible" to the user. Right: Expected patterns of results when modelling perception as a function of actual impact location. Unlike the other two hypotheses embodiment predicts that impact localisation will manifest as a linear function (blue line) for the entire body of the tool, mirroring what we observe for tactile localisation on a body part. **(c)** Three phases composed each trial, including object contact (top row) and localisation with the cursor (red circle; bottom row). **(d)** Group level affine regressions for Experiment 1 (n=10). Dashed lines correspond to the 95% confidence interval. The grey line corresponds to the equality line. **(e)** Slope for each participant from Experiments 1–5 (n=60). The distalisation model's prediction (i.e., chance performance) is shown by the orange line. **(f)** Model comparisons (AIC-difference: Projected - Embodiment) for every participant in Experiments 1–5 (n=60). The majority of comparisons favoured sensory embodiment (blue) with substantially less either favouring sensory projection (purple) or providing equivocal evidence (grey). **(g)** Experiment 6 (n=10): Participants failed to differentiate between distinct locations when contact was made with the rod's non-rigid portion (purple; unpredictable dynamics). In contrast, localisation had a positive slope when contact was made with the rigid portion (green; predictable dynamics). **(h)** Judgments shown in **g** were above the equality line because participants overestimated the contribution of the rigid portion to the rod's overall length (76.3% ± 4.8). Judgments overlapped with the equality line (gray) when normalised to the felt rigid-to-length ratio. Error bars in **g** and **h** correspond to one s.e.m.

When using a rod to manipulate an object, do humans perceive *where* the object contacts its surface? Several distinct patterns may characterise perception during tool-mediated sensing (Fig. 1b). First, based upon a longstanding hypothesis (*sensory distalisation*)[10], localisation may be confined to the tip of the rod regardless of the actual contact location. Alternatively, localisation may be "projected" to the proximal and distal regions of the rod (*sensory projection*), following the known deployment of spatial attention along a tool[11]. We combine multiple lines of evidence to characterise how humans use a tool to extend somatosensory processing.

When measuring tactile localisation, it is common to require participants to indicate on a graphical representation of a limb where they were touched[20]. We adapted this task to the case of hand-held

wooden rods (see Methods; Fig. 1b, Extended Fig. 1a). Participants localised impacts (seven distinct locations) on a downsized graphical representation of a rod, a task that requires mapping tactile signals within a coordinate system that is intrinsic to the space of the tool and not the external space it occupies. Localisation occurred following contact with an object through either self-generated action (*active sensing*) or passive reception of impact (*passive sensing*). Comparing these sensing modes let us infer the roles of sensory and motor signals in the perception of impact location.

In all experiments, we used affine regression to assess localisation performance. The slope reflects the perceived separation between landmarks and is therefore a measure of performance. Our analysis compared estimated slopes to random (slope: 0.25) and 'ideal' localisation (slope: 1). In doing so, we could test each hypothesis of tool-mediated sensing as only sensory embodiment predicts accurate localisation. We further adjudicated between sensory embodiment and projection (Fig. 1b) by comparing the Akaike information criterion of each model (ΔAIC) for each participant.

In an initial experiment (n=10) participants used both sensing modes (order counterbalanced) following a five-minute familiarization phase. Active sensing produces a rich array of motor (e.g., efference copies) and transient sensory signals (e.g., cutaneous vibrations) that could be used to extract impact location. Localisation during active sensing was highly accurate (slope: 0.93±0.09; one-sample t-test versus random: P<0.001; Fig. 1d), reflecting near-ideal performance (versus 1: P=0.46). Compared to active sensing, passive sensing largely removes motor-related signals while preserving most of the sensory signals. Participants consistently underestimated the distances between impact locations (slope: 0.57±0.04), as expected when informative cues are removed[21]. Nevertheless, performance during passive sensing was still accurate (versus random: P<0.005), though substantially lower than in the active condition (paired t-test: P<0.005). These results clearly favour sensory embodiment over distalisation.

Follow-up experiments provided a more complete picture of extended sensing (Extended Table 1). To demonstrate the robustness of our initial findings, we replicated them for both active (Extended Fig. 2a) and passive sensing (Extended Fig. 2b). In a fourth experiment, we found that participants localised contact on a rotated drawing with equal accuracy as when the drawing was displayed parallel to the rod (paired t-test: P=0.44; correlation: r=0.89; Extended Fig. 2c-e), providing further evidence that users internally represent the rod in tool-centred coordinates.

Finally, we probed the importance of sensorimotor predictions for extended sensing[9]. In a fifth experiment, we found that accurate location sensing did not depend on prior experience wielding the rod (Extended Fig. 2f), likely because the adult nervous system has internal mechanisms for predicting the structural dynamics of wooden rods. To link these dynamics to impact location, however, the nervous system must assume that the rod is uniformly rigid (see Supplementary Data). We violated this assumption in a sixth experiment by requiring participants to wield a rod whose handle and first half was rigid (wood) and second half was non-rigid (foam; Extended Fig. 1b). Prior to the localisation task, users held the rod by its handle but never saw or wielded it. The structural dynamics of its wooden half were therefore predictable, whereas they were unpredictable for the foam half (Extended Fig. 2g). Accurate localisation was impossible when contact was on the foam half (Fig. 1g). In contrast, users accurately rescaled their localisation on the wooden half (Fig. 1g-h), demonstrating that the nervous system adapts its expectations about dynamics when novel tools violate the rigidity assumption.

Our behavioural experiments converged to a similar conclusion. Almost every participant's performance was above chance (Fig. 1e), ruling out the sensory distalisation model. Furthermore, sensory embodiment was the significantly better model than sensory projection in the vast majority of datasets (54/70 versus 3/70; mean ΔAIC: 7.62±0.76; Fig. 1f). These results are in line with the predictions of sensory embodiment and provide strong evidence that tools function as sensory extensions of the body.

The high accuracy observed in each experiment demonstrates that sensory embodiment is largely independent of sensing mode. The differences between active and passive sensing do, however, have implications for the information used during extended sensing. Superior performance during active sensing (Extended Fig. 2g) suggests that human tool-users utilize information encoded in both sensory and motor signals[8]. Nevertheless, the remarkably high accuracy during passive sensing suggests that sensory signals, alone, encode a substantial portion of spatial information.

How does a tool communicate impact location to the hand? Tactile mechanoreceptors in the human hand[22] are highly sensitive to the cutaneous vibrations[23] elicited during object manipulation. According to the Euler-Bernoulli beam theory, a rod resonates according to well-defined modes when contacting an object (Supplementary Data Section 1). Crucially, the relative amplitude and phase of each mode depends almost exclusively on *where* contact occurs along the rod, relative to its length (Fig. 2a; Extended Fig. 3). The modal response thus encodes an invariant signal of location[24], suggesting that rods are a highly robust means to extend somatosensory processing provided that users can predict key aspects of their material and geometry (Experiments 5–6). We therefore hypothesized that during tool-extended sensing, a rod mechanically transduces impact location into *vibratory motifs* (Fig. 2a-b) that are decoded by the somatosensory system.

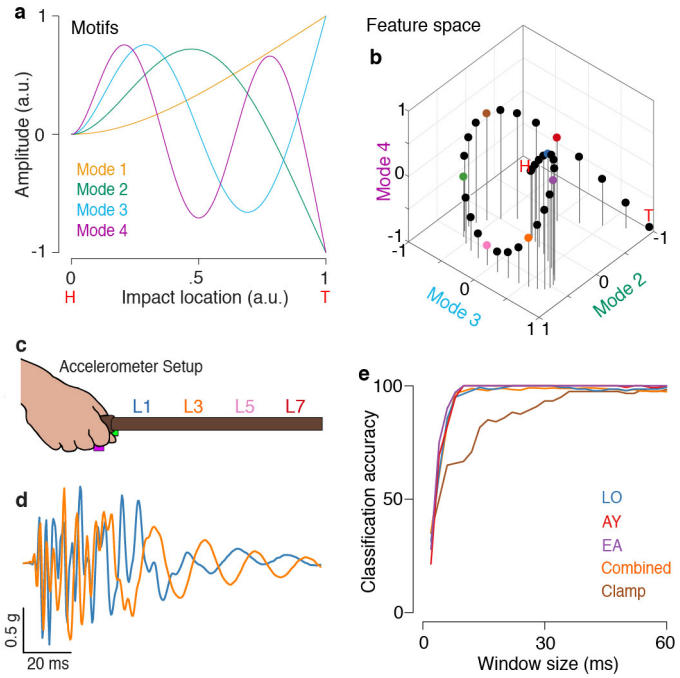

Figure 2. Vibratory motifs emerge rapidly during extended location sensing
(a) The amplitude of the first through fourth resonant modes as a function of impact location (see Supplementary Data). Impact at each location along the rod produces a unique combination of modal amplitudes, which we term *vibratory motifs*. **(b)** Hypothetical feature space of motifs constructed from the modes shown in **a**. The geometry of this space is, theoretically, identical for all uniform rods used by humans. Impact at any location (circles) from the handle (H) to tip (T) produces a motif that is situated in a unique position within the feature space. The coloured dots correspond to the impact locations used in our experiment. **(c)** Vibrations on the tool (green) and index finger (purple) were measured simultaneously following impacts at seven distinct locations (L1–L7). **(d)** Motifs from EA's dataset for L1 and L3. Similar patterns were observed for LO and AY. **(e)** The accumulation of location information within motifs was rapid for each participant and when all datasets were combined (orange), demonstrating that each participant's motifs share location-specifying features. All cases rivalled what was observed for vibrations when the tool was fully clamped (brown; see pilot experiment in Supplementary Data Section 3), suggesting that the information encoded by motifs is strengthened by the biomechanical properties of the hand.

We recorded vibrations on the handle of a rod and the index finger of three human participants while they performed either passive (participants LO and AY) or active (participant EA) extended sensing (Fig. 2c; Extended Fig. 1c). Behavioural results for each participant were within the range observed

previously (Extended Fig. 2i). Impact at each location produced distinct vibratory motifs (Fig. 2d) that were highly consistent across trials (Extended Fig. 4). Support vector classification found that the location-specific pattern of each motif emerged extremely rapidly, with classification accuracy reaching 90% within ~8 ms post-impact (Fig. 2e). High classification accuracy was also found for patterns of a motif's phase-locked temporal encoding (Extended Fig. 5a-c), a subspace of the modal response whose analysis is computationally efficient and neurophysiologically plausible (Supplementary Data Section 2). Similar results were found for cutaneous vibrations (Extended Fig. 6). Vibratory motifs are therefore an informationally rich signal that is likely exploited during tool-extended sensing.

What message does a tool send to its user's brain? Our findings thus far provide evidence that a rod's modal response reflects the initial transduction of information about impact location. This finding is comparable to object localisation during whisking by rats, where it has been suggested that information is initially processed *pre-neuronally* by the mechanics of the whiskers[2]. If vibratory motifs are to guide behaviour, mechanoreceptors in the hand must transduce them into neural response patterns that preserve the location-specifying information, a large portion of which is carried by a motif's phase-locked encoding (Extended Fig. 5). Pacinian mechanoreceptors are good candidates for this transformation given their broad frequency tuning[25], temporally precise spiking[26], and phase-locked response properties[27]. They have been proposed to play an important role in encoding vibrations transmitted through hand-held objects[5]. We leveraged a biologically plausible skin-neuron model of the hand (TouchSim)[12] to simulate how impact location may be re-encoded by mechanoreceptors during extended sensing.

We simulated the spiking responses of a population of forty-two Pacinian mechanoreceptors (Fig. 3a) to the mechanical vibrations described above. Simulated spikes showed a temporally precise phase-locked relationship with the motifs (Fig. 3b; Extended Fig. 5a-b). The population response started 6.2±0.8 ms post-impact, suggesting that pre-neuronal and neuronal representations of object location co-evolve in time. Importantly, substantial location information emerged in the population's response within ~25 ms (Fig. 3c) and was dependent upon the millisecond precision of spiking (Fig. 3c, inset; Extended Fig. 7). This time course is in line with the responses of mechanoreceptors during object manipulation with the hand[28], suggesting that the nervous system can extract sensory information from a tool with a similar speed as the body itself. Pacinian mechanoreceptors may therefore reduce the dimensionality of motifs while preserving information about impact location (see Supplementary Data Section 2).

Each participant's trial-by-trial judgments were predicted surprisingly well from the corresponding simulated population spiking pattern (multivariate regression with forty predictors: all R^2>0.8; all *predictive*-R^2>0.6; Fig. 3d; Extended Table 2), which provided significantly better fits than firing rate (Extended Fig. 8). Similar results were found when motifs were instead used as predictor variables (Fig. 3e; Extended Fig. 5d). Furthermore, both spike-timing and motifs accurately predicted the trial-by-trial directional errors (all R^2>0.75; all *predictive*-R^2>0.55), further underscoring their importance for behaviour.

In conclusion, we have provided behavioural, mechanical, and computational evidence that humans utilise tools as sensory extensions of the body. Our results suggest that the human nervous system contains finely tuned mechanisms for decoding vibratory motifs, including sensorimotor internal models that can anticipate the structural dynamics of rods[9,29]. Object localisation with a rod therefore represents an important human model of extended sensing[1], where information processing is distributed across the mechanical response of the tool, the biomechanics of the extremities, and the neural circuits of the sensory-motor system[13]. Morphological and neural changes in the hand during human evolution[30] may reflect selection pressure to maximize the functional coupling and embodiment of tools[16].

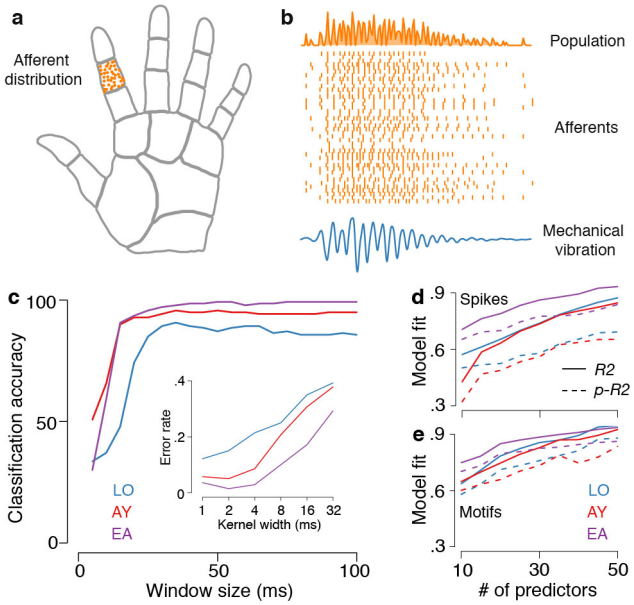

Figure 3. Impact location is encoded in the spike-timing of tactile mechanoreceptors in the hand **(a)** The distribution of forty-two simulated Pacinian mechanoreceptors in the middle phalanx of the index finger. This image has been produced using TouchSim[12]. **(b)** Mechanical vibration (first 150 ms post-impact) on a randomly chosen trial from LO's dataset. Vibrations led to temporally precise response patterns across the individual afferents (orange raster plot) and the population response (top). **(c)** We could accurately decode impact location from the population spike-timing. (Inset) The classification error rate increased dramatically for kernel widths greater than four milliseconds. **(d-e)** Model fits for each participant's behaviour as a function of the number of predictors (140 data points per test): **(d)** Spikes and **(e)** Motifs. Solid lines correspond to R^2 and dashed lines correspond to *predictive-*R^2.

Acknowledgments

This work was supported by an FRM postdoctoral fellowship to L.E.M., from ANR-16-CE28-0015 Developmental Tool Mastery to A.F. and V.H., by a Leverhulme Trust Visiting Professorship Grant to V.H., and from IHU CeSaMe ANR-10-IBHU-0003, Defi Auton Sublima, and the James S. McDonnell Scholar Award to A.F. All work was performed within the framework of the LABEX CORTEX (ANR-11-LABX-0042) of Université de Lyon. We thank Frédéric Volland for his help constructing the experimental setup. We would also like to thank Blake Miller and Andrew Schork for their statistical advice, as well as Lisa Quadt, Alice Roy, Eric Leonardis, and Konstantina Kilteni for their feedback on an earlier version of the manuscript.

Author contributions

L.E.M., V.H., and A.F. conceived the study and designed the experiments. L.E.M. and L.M. collected and analysed the behavioural experiments. E.K. and R.S. constructed equipment for the vibration experiment and helped process the data. L.E.M., V.H., and A.F. designed and analysed the neuronal modelling and vibration experiments. V.H. developed the theoretical framework presented in the Supplementary Data. L.E.M., V.H., and A.F. wrote the paper. All authors approved the final version of the paper.

Author information

The authors declare no competing financial interests. All data has been archived at the Open Science Framework (https://osf.io/283cq/). Correspondence and request for materials should be addressed to luke.miller@inserm.fr or alessandro.farne@inserm.fr.

1. Clark, A. & Chalmers, D. The extended mind. *Analysis* **58.1,** 7–19 (1998).
2. Bagdasarian, K. *et al.* Pre-neuronal morphological processing of object location by individual whiskers. *Nat. Neurosci.* **16,** 622–631 (2013).
3. Japyassú, H. F. & Laland, K. N. Extended spider cognition. *Anim. Cogn.* **20,** 375–395 (2017).
4. Chan, T. C. & Turvey, M. T. Perceiving the vertical distances of surfaces by means of a hand-held probe. *J. Exp. Psychol. Hum. Percept. Perform.* **17,** 347–358 (1991).
5. Brisben, A. J., Hsiao, S. S. & Johnson, K. O. Detection of Vibration Transmitted Through an Object Grasped in the Hand. *J Neurophysiol* **81,** 1548–1558 (1999).
6. Klatzky, R. L. & Lederman, S. J. Tactile roughness perception with a rigid link interposed between skin and surface. *Percept. Psychophys.* **61,** 591–607 (1999).
7. Yamamoto, S. & Kitazawa, S. Sensation at the tips of invisible tools. *Nat. Neurosci.* **4,** 979–980 (2001).
8. Saig, A., Gordon, G., Assa, E., Arieli, A. & Ahissar, E. Motor-Sensory Confluence in Tactile Perception. *J. Neurosci.* **32,** 14022–14032 (2012).
9. Kilteni, K. & Ehrsson, H. H. Sensorimotor predictions and tool use: Hand-held tools attenuate self-touch. *Cognition* **165,** 1–9 (2017).
10. Katz, D. *The world of touch*. (Erlbaum, 1989; original work published in 1925).
11. Holmes, N. P., Calvert, G. A. & Spence, C. Extending or projecting peripersonal space with tools? Multisensory interactions highlight only the distal and proximal ends of tools. *Neurosci. Lett.* **372,** 62–67 (2004).
12. Saal, H. P., Delhaye, B. P., Rayhaun, B. C. & Bensmaia, S. J. Simulating tactile signals from the whole hand with millisecond precision. *Proc. Natl. Acad. Sci.* **114,** E5693–E5702 (2017).
13. Chiel, H. J. & Beer, R. D. The brain has a body: Adaptive behavior emerges from interactions of nervous system, body and environment. *Trends Neurosci.* **20,** 553–557 (1997).
14. Makin, T. R., De Vignemont, F. & Faisal, A. A. Neurocognitive barriers to the embodiment of technology. *Nat. Biomed. Eng.* **1,** 1–3 (2017).
15. Johnson-Frey, S. H. The neural bases of complex tool use in humans. *Trends Cogn. Sci.* **8,** 71–78 (2004).
16. Martel, M., Cardinali, L., Roy, A. C. & Farnè, A. Tool-use: An open window into body representation and its plasticity. *Cogn. Neuropsychol.* **33,** 82–101 (2016).
17. Miller, L. E., Longo, M. R. & Saygin, A. P. Tool morphology constrains the effects of tool use on body representations. *J. Exp. Psychol. Hum. Percept. Perform.* **40,** 2143–2153 (2014).
18. Descartes, R. *La Dioptrique (1637)*. (Œuvres et lettres, 1987).
19. Schenkman, B. N. & Jansson, G. The Detection and Localization of Objects by the Blind with the Aid of Long-Cane Tapping Sounds. *Hum. Factors* **25,** 607–618 (1986).
20. Mancini, F., Longo, M. R., Iannetti, G. D. & Haggard, P. A supramodal representation of the body surface. *Neuropsychologia* **49,** 1194–1201 (2011).
21. Kersten, D., Mamassian, P. & Yuille, A. Object Perception as Bayesian Inference. *Annu. Rev. Psychol.* **55,** 271–304 (2004).
22. Johnson, K. O. The roles and functions of cutaneous mechanoreceptors. *Curr. Opin. Neurobiol.* **11,** 455–461 (2001).
23. Shao, Y., Hayward, V. & Visell, Y. Spatial patterns of cutaneous vibration during whole-hand haptic interactions. *Proc. Natl. Acad. Sci.* **113,** 201520866 (2016).
24. Hayward, V. Haptic shape cues, invariants, priors and interface design. *Hum. Haptic Percept. Basics Appl.* 381–392 (2008). doi:10.1007/978-3-7643-7612-3_31
25. Bell, J., Bolanowski, S. & Holmes, M. H. The structure and function of pacinian corpuscles: A review. *Prog. Neurobiol.* **42,** 79–128 (1994).
26. Mackevicius, E. L., Best, M. D., Saal, H. P. & Bensmaia, S. J. Millisecond Precision Spike Timing Shapes Tactile Perception. *J. Neurosci.* **32,** 15309–15317 (2012).
27. Talbot, W. H. & Mountcastle, B. The Sense of Flutter-Vibration : the Human the Monkey of Mechanoreceptive Comparison of Capacity With Response Patterns Aff erents From. *J. Neurophysiol.* **31,** 301–334 (1968).
28. Johansson, R. S. & Birznieks, I. First spikes in ensembles of human tactile afferents code complex spatial fingertip events. *Nat. Neurosci.* **7,** 170–177 (2004).
29. Imamizu, et al. Human cerebellar activity representing acquired internal model of a new tool. *Nature* **403,** 192–5. (2000).
30. Young, R. W. Evolution of the human hand : the role of throwing and clubbing. *Journal of Anatomy* **202,** 164–174 (2003).

Methods

Participants

Sixty-three participants in total completed our behavioural experiments: Ten in Experiment 1 (9 right-handed, 4 males, 27.2±3.1 years of age), ten in Experiment 2 (10 right-handed, 5 males, 27.8±2.6 years of age), ten in Experiment 3 (9 right-handed, 4 males, 26.5±2.5 years of age), twenty in Experiment 4 (all right-handed, 12 males, 22.6±2.1 years of age), and ten in Experiment 5 (9 right-handed, 7 males, 29.1±2.7 years of age); these same ten participants also completed Experiment 6 (order counterbalanced). A further three right-handed participants completed a more in-depth psychophysical experiment: LO (female; 24 years of age), AY (female; 25 years of age), and EA (male; 20 years of age). All participants had normal or corrected-to-normal vision and no history of neurological impairment. Every participant gave informed consent to participate in the experiment. The study was approved by the ethics committee (CPP SUD EST IV, Lyon, France).

Apparatus and impact localisation task

The setup for each behavioural experiment (Extended Fig. 1a) was as follows: Participants were either seated comfortably in a cushioned chair (Experiments 1–4, and 7) or standing in a comfortable posture (Experiments 5 and 6). Their right arm was placed in a padded arm rest and hidden from view with a long occluding board. An LCD screen (47 x 30 cm) lay backside down nine cm from the edge of the table and in the length-wise orientation (centred on the participant's midline). This orientation allowed us to display a long computer drawing of the tool that was viewed by the participants during the task (see below).

Several types of wooden rods were used in the experiments. Their details are as follows: In Experiments 1–3 and 7, the wooden rod (Byron & Byron; Model: tiara draw rod) had a 10-cm handle and an 83-cm body (0.6 cm radius). In Experiment 4 the wooden rod had a 12-cm handle and a 60-cm body (0.75 cm radius). In Experiment 5 the wooden rod had a 12-cm handle and an 83-cm body (0.75 cm radius) that was insulated from handle-to-tip with a lightweight foam covering. In Experiment 6, we used a hybrid tool that was ~half rigid and ~half non-rigid. The rigid portion of the rod was wood with 12-cm handle and a 38-cm body (0.75 cm radius). As before, the rod was insulated with a lightweight foam material that covered both the wooden portion and extended a further 45-cm, thus forming a non-rigid portion. The dynamics of each half were therefore very different, with only the rigid portion being predictable to the participant, given that it was the only portion they were exposed to prior to wielding (see below). The rod was held in the participant's right (Experiments 1–4 and 7) or dominant hand (Experiments 5–6) and was always fully blocked from view by the occluding board.

The task in each experiment was to localise where an object contacted the surface of the tool by pointing to the corresponding location on the graphical representation of the tool. This drawing was scaled to 40% of the rod's actual dimensions; it began 14.5 cm from the edge of the table and was raised 4 cm above the table surface. A red cursor (0.2 cm radius) was placed 10 cm to its right. The drawing was displayed in parallel with the actual rod in all experiments except Experiment 4. In this experiment, the drawing of the rod was rotated 90-degrees counter-clockwise on half of the trials (randomly interleaved with the parallel drawings). This manipulation allowed us to more rigorously characterise how the rod is internally represented. If localisation performance is independent of drawing orientation, that would provide strong evidence that the rod is represented in a tool-centred coordinate system. Indeed, debriefing interviews after the experiment found that most participants found both orientations as equally challenging. While it cannot be completely ruled out that localising on the rotated drawing was done using explicit mental rotation, it is unlikely since that the majority of participants reported that the task required little effort or attention to switch between response modes (i.e., upright and rotated).

In most experiments (1–3 and 5–7) there were seven distinct impact locations (i.e., landmarks), ranging from 13 to 73 cm from the handle (by steps of 10 cm). In Experiment 4 there were six distinct

landmarks, ranging from 10 to 60 cm from the handle (by steps of 10 cm). This information was never given to participants. There were 10 trials per landmark in the first six experiments (70 trials total) and 20 trials per landmark in the final experiment (140 trials total). The specific landmark for each trial was chosen pseudo-randomly.

The object used to contact the rod in the first six experiments was a wooden block (3 cm width) with a tightly wrapped wool padding (~3.5 cm contact area) to minimize the sound of impact. The objects used in the final experiment were a narrow plastic stick (0.2 cm width) for two participants (LO and AY) and a wooden block (3 cm width) for one participant (EA). To further minimize auditory cues during the task, pink noise was played over headphones. Pilot studies confirmed that residual auditory cues were minimal and uninformative about impact location.

Our experiments tested two distinct types of sensing impact location: *Active* sensing (Experiments 1, 2, and 4–7) and *passive* sensing (Experiments 1, 3, and 7). During active sensing, the participant wielded the tool into contact with the object. They were instructed to briefly tap the object a single time and not rest the tool on it, meaning that active wielding required both self-generated active and reactive movements. During passive sensing, the experimenter manually moved the object into contact with the tool, transferring mechanical energy into the tool's body that was passively received by the participant. The only tool movements in this sensing mode were passively reactive. In Experiment 1, where each participant sensed both actively and passively, each sensing mode occurred in distinct blocks (order counterbalanced across participants).

Experiments 1–4 and 7 began with a sensorimotor familiarization session. During this session, participants were told to explore how the tool felt to contact a surface (padded edge) at different locations on the tool. Emphasis was placed on the vibratory aspect of the contact. Participants had full auditory and visual feedback throughout this familiarization session, which was self-paced and lasted for five minutes. Next, these participants were given a brief practice session (seven trials) with the localisation task to familiarize themselves with the trial structure (see below). The actual localisation task commenced following this practice session.

In contrast, there was no sensorimotor familiarization or practice sessions in Experiments 5 and 6. Instead, participants were handed the rod only after the experiment was ready to commence, beginning the actual localisation task roughly two minutes after they were given the rod. At no time did they ever see or hear the rod. Only somatosensory feedback about the rod's material and geometry was available. This allowed us to test whether *specific* familiarity with the rod was necessary for accurate localisation, or whether participants could use general knowledge about the dynamics of rods to sense impact location (see Supplementary Data).

The trial structure in each experiment was as follows: In the 'Pre-contact phase', participants sat with their left hand on a trackball, their trunk centred on the drawing of the tool, and their right hand holding the tool situated behind the occluding board. A red cursor (circle, 0.2 cm radius) was placed 10 cm to the right of the tool drawing. A 'go' cue (tap on the right shoulder) indicated start of the 'Contact phase'. They therefore had to either move the tool into contact with the object (active sensing; Experiments 1, 2, and 4–7) or wait passively to sense the impact (passive sensing; Experiments 1, 3, and 7), which occurred approximately one second following the 'go' cue. In the final phase of the trial—the 'Localisation phase'—participants made their judgment about impact location. This was done by moving the cursor onto the graphical representation of the tool corresponding to the impact location and clicking the mouse. The drawing then briefly disappeared for 500 ms before reappearing in the same position, indicating the beginning of the next trial. Participants never received feedback about their performance or the correct impact location.

Participants used a "hybrid" rod in Experiment 6 (see above for details). At the end of the experiment, participants used a tape measurer to report the felt length of the rigid and non-rigid portion separately. A debriefing interview following the experiment found that participants were confident in the length and material of the wood portion. Given that only somatosensory information about the material from the handle was available to participants in Experiment 6, as far as they knew the rod was only made

of wood—post-experiment interviews showed that this was indeed the belief of every participant at the beginning of the experiment. They were therefore unsure of what the non-rigid portion of the rod was made of and used a purely cognitive strategy to infer that contact on its surface must be farther than the tip of the wood portion.

Vibration recording apparatus and experiments

We hypothesised that information about impact location would be encoded by the modal response of the rod when contacted. Vibrations were recorded using miniature tri-axis analogue accelerometers (Analog Devices; Model ADXL335). These devices have low mass (40.0 mg), wide frequency bandwidth (0–1,600 Hz in X and Y; 0–550 Hz in Z), and high dynamic range (−3.6 to 3.6 g). The signals were digitized with a 14-bit resolution and sampled at a frequency of 2.5 kHz over a five-second window using a data acquisition device (National Instruments; Model USB-6009). Recording was restricted to the Z-axis as this contained the bulk of the impact response. Adhesive tape was used to keep the accelerometers in place on the surface of interest. For participants LO and AY, a single accelerometer was attached to the handle of the tool and one to the middle phalanx of the index finger (D2m; dorsal surface) and vibrations were recorded from each surface simultaneously. For participant EA, we decided to focus exclusively on mechanical vibrations. Therefore, a single accelerometer was attached to the base of the tool shaft. All data was recorded and processed using Matlab 2016b (The MathWorks).

Vibration Experiment: Tool held in the hand

The goal of this experiment was to investigate whether location information was encoded in mechanical vibrations during tool sensing (Extended Fig. 1c). Vibrations were recorded while participants passively (LO and AY) or actively (EA) sensed impact location. The behavioural task was identical to the behavioural experiments with the exception that there were twenty trials per each of the seven locations. In the passive sensing condition, each participant was trained to hold the tool as still as possible and with a similar grip force across trials. Great care was taken by the experimenter to ensure that this object contacted the tool with a similar force across trials. Recordings made directly from the tool occurred at its base and approximately two centimetres proximal from the beginning of the handle. The index finger was placed directly behind this accelerometer. In the active sensing condition, EA was trained to hold the tool with a stable grip force when resting and to contact the object with as similar of force as possible across all trials. Vibrations were recorded from a single accelerometer placed at the base of the tool shaft one cm distal to the handle. We set a minimum ten-second interval between each trial to ensure that all vibrations had fully dampened.

Signal processing

We used the following steps to process the vibrations recorded on each trial of every experiment: First, we converted the signal from voltage into a unit of acceleration, g=9.81 m/s^2. Second, we filtered the signal using a zero-phase FIR filter with a bandpass between 100–600 Hz. This specific bandpass was chosen because it isolated the second through fourth modes (Fig. 2a-b), it served to remove most of the motor components from the accelerometer readings, and pilot studies indicated that it best captured location information. Third, we aligned the onset of vibrations to the time-point zero and cut the signal with a window of -100 to 300 ms post-impact. Fourth, we used mean-subtraction to remove the baseline from the signal.

Skin-neuron model

We used a biologically plausible computational skin-neuron model[12] (TouchSim) to simulate putative mechanoreceptor responses in the hand during tool-mediated sensing. Matlab code to implement the model is freely available online (http://bensmaialab.org/download/). The reader should refer to the original article for an in-depth treatment of the methods. Briefly, TouchSim simulates the spiking response and the spatial distribution of three different types of tactile afferents in the volar region of the hand: slow-adapting type one, rapidly adapting, and Pacinian. The responses for each afferent type

to a given stimulus are determined in two sequential stages: First, both the local deformation of the skin (static component) and the propagation of surface waves across the hand (dynamic component) are estimated. Second, this spatiotemporal pattern of stresses is used as input into afferent-specific integrate-and-fire models to determine the spiking response to the given stimulus. The model parameters of each afferent were derived from spiking data obtained in monkeys. The simulated responses of afferents closely match the known spiking responses (both millisecond precise spike-timing and rate) of actual afferents to various classes of stimuli (e.g., vibrations, edges, textured surfaces).

We modelled the responses of a population of Pacinian afferents to the mechanical vibrations measured in the vibration experiment. The population was composed of forty-two realistically distributed afferents in D2m; we confined our population to D2m as this was adjacent to where vibrations were measured from the handle. The response profile of each afferent was binned with a one-millisecond resolution, allowing us to investigate its spike-timing with high temporal precision. To more realistically simulate afferents, the temporal profile of their responses included stochastic noise and considered known mechanical and spiking delays. Population-level spiking was created by summing the spiking of each individual afferent. The rate code for each afferent was calculated as its firing-rate over time.

The mechanical vibration dataset for each participant (LO, AY, and EA) was used as input for the model. Double integration with the trapezoidal method was used to convert acceleration (m/s^2) into displacement (μm). A zero-phase FIR filter with a high-pass at 80 Hz removed any accumulation of low-frequency error in the signal during this process. The time window of each vibration was restricted to 0 to 150 ms post-impact. The modelled stimulus area had a radius of 7 mm and an indentation of 2 mm and was centred on D2m. This size roughly approximates the actual stimulus area when grasping a tool. Virtually identical results were found for a stimulus area with a radius of 3 mm (data not shown).

Data analysis

Behavioural analysis

To assess a participant's ability to localise impact location on a tool, the mean localisation judgement for each of the landmarks was fit with a least-squares affine regression. The decision to fit our data with a linear model was made prior to collecting data and was because non-linear models did not provide better fits in pilot experiments. The judged impact location on the drawing was converted from pixels into 'centimetres', i.e., tool space, and was modelled as a function of actual impact location. The slope of the regression was used as our main measure of localisation ability, although identical results are found when analysing the intercept.

To first assess whether the slope was greater than expected by chance (as is predicted by the sensory distalisation model), we created a bootstrapped distribution of the slopes of regressions fit to simulated datasets of random guesses (100,000 simulations). The upper 95% confidence interval of this distribution (i.e., 5000^{th} highest ranked element) was a slope of 0.25; A one-sample *t*-test was used to compare the actual slopes to this value. Next, to assess whether performance was 'near ideal', we used a one-sample *t*-test to compare the actual slopes to 1 (i.e., the equality line) and the actual intercepts to 0. Paired *t*-tests were used in Experiments 1 and 4 to compare performance in the within-subject conditions. All statistical tests were two-sided.

We further fit every participant's data (first five experiments) with the predicted pattern of results from the sensory projection model (Fig. 1b, right inset). For Experiment 4, this was modelled as a proximal judgment of 10 cm for contact at the first three landmarks (actual location: 10, 20, and 30 cm) and a distal judgment of 60 cm for contact at the last three landmarks (actual location: 40, 50, and 60 cm). For all other experiments, this was modelled as a proximal judgment of 13 cm for contact at the first three landmarks (actual location: 13, 23, and 33 cm) and a distal judgment of 73 cm for contact at the last four landmarks (actual location: 43, 53, 63, and 73 cm). Akaike information criterion (AIC) was used to compare the fit of the sensory projection model with that of the sensory embodiment model (i.e., the equality line in a linear regression; Fig. 1b, right inset). The model with the lower AIC score

provides a better fit to the data. A significance cut off for the difference between fits (ΔAIC) was set to 3.22, which means that the better model is five times more likely to explain the pattern of judgments than the worse model.

In Experiment 6, we sought to determine whether participants accurately rescaled their internal map of the rod to their estimated rigid to non-rigid ratio. All participants except one reported that the rod had both a rigid and non-rigid part and all participants over-estimated the actual contribution of the rigid portion to the rod's overall length (0.76 ± 0.05). We hypothesised that a rescaling of this map would manifest itself as an over-estimation (i.e., above the equality line) of where on the drawing they localised impacts on the rigid portion. Each participant's proportion estimate was used to normalise their localisation judgments to compare the actual and ideal pattern of rescaling.

Analysis of vibrations

We first investigated whether impact at distinct locations on a tool led to highly reproducible vibration patterns, termed *vibratory motifs*. We measured the cross-correlation between every possible unique pairwise comparison for vibrations (time window: 0–100 ms) within each location (190 per location, 1330 in total). This was done separately for each surface and for each participant. The distribution of values was characterized by taking the median cross-correlation value and the interquartile range.

We next classified impact location from vibratory motifs using a support vector machine[31] (SVM) with a radial basis kernel. Our classification scheme used 5-fold cross validation. Thus, we trained the classifier on four subsamples of the data (i.e., 80% of the trials) and tested classifier performance on the leftover subsample (i.e., the remaining 20% of the trials). Each fold had an equal number of items per impact location. The hyperparameters of the SVM, C and γ, were tuned using grid search; tuning occurred separately for each of the five classification iterations. We specifically sought to characterize when a location-specific pattern emerged in the rod's modal response. The features for classification were therefore subsets of the modal response across multiple temporal window sizes (2 to 60 ms, in steps of 2 ms). Classification was performed using the e1071 package[32] and its interface with LIBSVM[33]. This was implemented with R version 3.2.3.[34]. Chance classification (i.e., random guessing) was ~14%.

Analysis of afferent responses

Impact location was classified from the summed millisecond-precise spiking of the entire PC population (0–100 ms post-impact). As before, we used an SVM (5-fold cross validation) for classification with hyperparameters that were tuned using grid search. The features for classification were subsets of the spiking response across multiple time window sizes (5 to 100 ms, by steps of 5 ms). These results can be thought of as providing a theoretical lower bound for the accumulation of location information in the nervous system. Chance classification was ~14%.

The coding of tactile information by the somatosensory system is often dependent upon the millisecond precise spiking of its first-order neurons[26,35-37]. To investigate whether impact location coding was dependent upon millisecond precision, we convolved the population-level spiking response on each trial with a Gaussian kernel at six distinct widths (1, 2, 4, 8, 16, and 32 ms). We then used an SVM to classify impact location from the first 50 ms of its response. This process was repeated for each of the six kernel widths and for each participant's dataset separately.

We further investigated whether trial-by-trial localisation can be modelled as a function of the corresponding putative spiking response of the PC population (0–150 ms post-impact) using multivariate regression. We initially focused exclusively on the spike-timing of the PC population (1 ms resolution). The FWDselect[38] package in R was used to select a range of time-points (ten to fifty predictor variables) that provided the best model fit as determined with Akaike information criterion (AIC; 5-fold cross validation). R^2 and root-mean squared error were used to assess the fit of the final model. Leave-one-out cross-validation was then used to assess the model's predictive power. The value for every trial was estimated with separate regression fit to the remaining 139 trials. We then

calculated a *predictive-R^2* from the relationship between estimated and actual behaviour. This procedure was done separately for each participant.

We next attempted to compare the ability of a spike-timing code and a rate code to model each participant's behaviour. We repeated the methods described above to model the trial-by-trial localisation as a function of the firing rate of each of the forty-two afferents. This was done for each participant separately. We compared the performance of the rate code and a spiking model (forty-two predictors) using AIC.

Data and code availability

All data has been archived at the Open Science Framework (https://osf.io/283cq/). Analysis code will be made available upon request to the corresponding authors, L.E.M. and/or A.F.

12 Saal, H. P., Delhaye, B. P., Rayhaun, B. C. & Bensmaia, S. J. Simulating tactile signals from the whole hand with millisecond precision. Proc Natl Acad Sci U S A 114, E5693-E5702, doi:10.1073/pnas.1704856114 (2017).

26 Mackevicius, E. L., Best, M. D., Saal, H. P. & Bensmaia, S. J. Millisecond precision spike timing shapes tactile perception. J Neurosci 32, 15309-15317, doi:10.1523/JNEUROSCI.2161-12.2012 (2012).

31 Cortes, C. & Vapnik, V. Support-vector networks. Machine learning 20, 273-297 (1995).

32 Meyer, D., Dimitriadou, E., Hornik, K., Weingessel, A. & Leisch, F. e1071: Misc Functions of the Department of Statistics, Probability Theory Group (Formerly: E1071), TU Wien. R package version 1.6-7. (2015).

33 Chang, C.-C. & Lin, C.-J. LIBSVM: a library for support vector machines. ACM Transactions on Intelligent Systems and Technology (TIST) 2, 27 (2011).

34 Team, R. C. R: A language and environment for statistical computing. Vienna, Austria: R Foundation for Statistical Computing. (2014).

35 Pruszynski, J. A. & Johansson, R. S. Edge-orientation processing in first-order tactile neurons. Nat Neurosci 17, 1404-1409, doi:10.1038/nn.3804 (2014).

36 Hayward, V. et al. Spatio-temporal skin strain distributions evoke low variability spike responses in cuneate neurons. Journal of the Royal Society, Interface 11, 20131015, doi:10.1098/rsif.2013.1015 (2014).

37 Jorntell, H. et al. Segregation of tactile input features in neurons of the cuneate nucleus. Neuron 83, 1444-1452, doi:10.1016/j.neuron.2014.07.038 (2014).

38 Sestelo, M., Villanueva, N. M., Meira-Machado, L. & Roca-Pardiñas, J. FWDselect: An R Package for Variable Selection in Regression Models. R package version 2.1.0. (2015)

Extended Data

Exp.	*Condition*	*Slope*	*Intercept*	R^2	*t-Test Type*	*Comparison*	*t*	*P*
*1**	Active	.93±.09	-2.20±2.01	.94±.02	One-sample	Slope vs. 0.25	7.82	<.001
						Slope vs. 1	0.77	.46
						Intercept vs. 0	1.09	.33
	Passive	.57±.04	14.18±3.3	.85±.02	One-sample	Slope vs. 0.25	7.08	<.001
						Slope vs. 1	9.75	<.001
						Intercept vs. 0	4.30	.002
					Paired	Slope	5.43	<.001
						Intercept	4.63	.001
*2**	Active	.94±.04	-1.13±2.72	.93±.01	One-sample	Slope vs. 0.25	16.04	<.001
						Slope vs. 1	1.48	.17
						Intercept vs. 0	0.41	.69
*3**	Passive	.77±.1	9.11±3.76	.87±.04	One-sample	Slope vs. 0.25	5.22	<.001
						Slope vs. 1	2.34	.04
						Intercept vs. 0	2.43	.04
*4***	Parallel	.95±.04	0.08±1.72	.91±.01	One-sample	Slope vs. 0.25	16.08	<.001
						Slope vs. 1	1.08	.29
						Intercept vs. 0	0.04	.97
	Rotated	.94±.05	-0.39±1.78	.92±.01	One-sample	Slope vs. 0.25	14.04	<.001
						Slope vs. 1	1.32	.20
						Intercept vs. 0	0.22	.83
					Paired	Slope	0.88	.44
						Intercept	0.53	.61
*5**	Active	1.13±.05	-4.30±3.38	.95±.01	One-sample	Slope vs. 0.25	19.40	<.001
						Slope vs. 1	2.84	.02
						Intercept vs. 0	1.27	.24

Extended Table 1. Behavioural results
*n=10; **n=20; Statistical tests were two-sided. Summary values are presented as mean ± s.e.m.

Participant[%]	*Sensing*	*Features*	$F_{42,97}$	R^2	*p*-R^2	*RMSE*	*AIC**
LO	Passive	Spike timing	11.04	0.83	0.65	7.20	1038.07**
		Rate	1.70	0.42	-0.22	13.13	1206.25
		Motifs	22.52	0.91	0.83	4.72	
AY	Passive	Spike timing	10.02	0.82	0.65	8.17	1073.46**
		Rate	1.62	0.45	-0.20	14.05	1225.16
		Motifs	17.9	0.89	0.77	6.38	
EA	Active	Spike timing	20.37	0.90	0.79	8.14	1072.55**
		Rate	1.73	0.37	-0.23	20.21	1327.09
		Motifs	26.85	0.92	0.85	7.18	

Extended Table 2. Multivariate models with forty-two predictor variables
[%]140 data points per regression; *p*-R^2=predictive-R^2; *RMSE*=root-mean squared error; *44 degrees of freedom per model. **Significantly better model

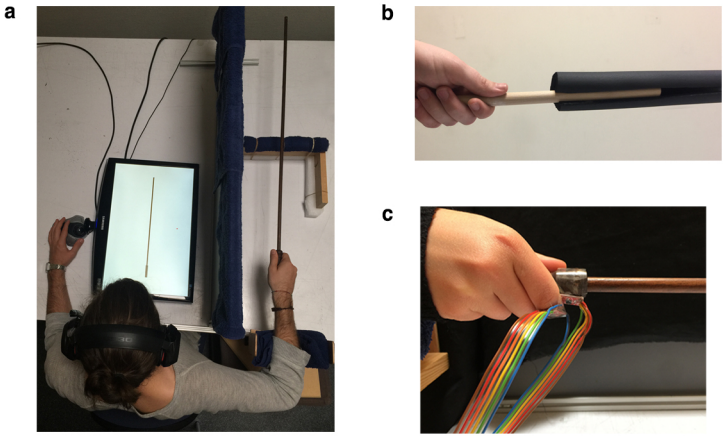

Extended Figure 1. Setup for the behavioural and vibration experiments
(a) The experimental setup for all behavioural experiments (see Methods for details). The object shown below the rod was used in the first three behavioural experiments. **(b)** The "hybrid" tool used in Experiment 6, which was half rigid (wood and insulation) and half non-rigid (insulation only). The foam is displayed as being open for presentation purposes only. The dimensions of the rod have also been altered for presentation purposes. See Methods for more details. **(c)** Setup for the vibration experiment, where accelerometers were attached to the handle and the participant's index finger.

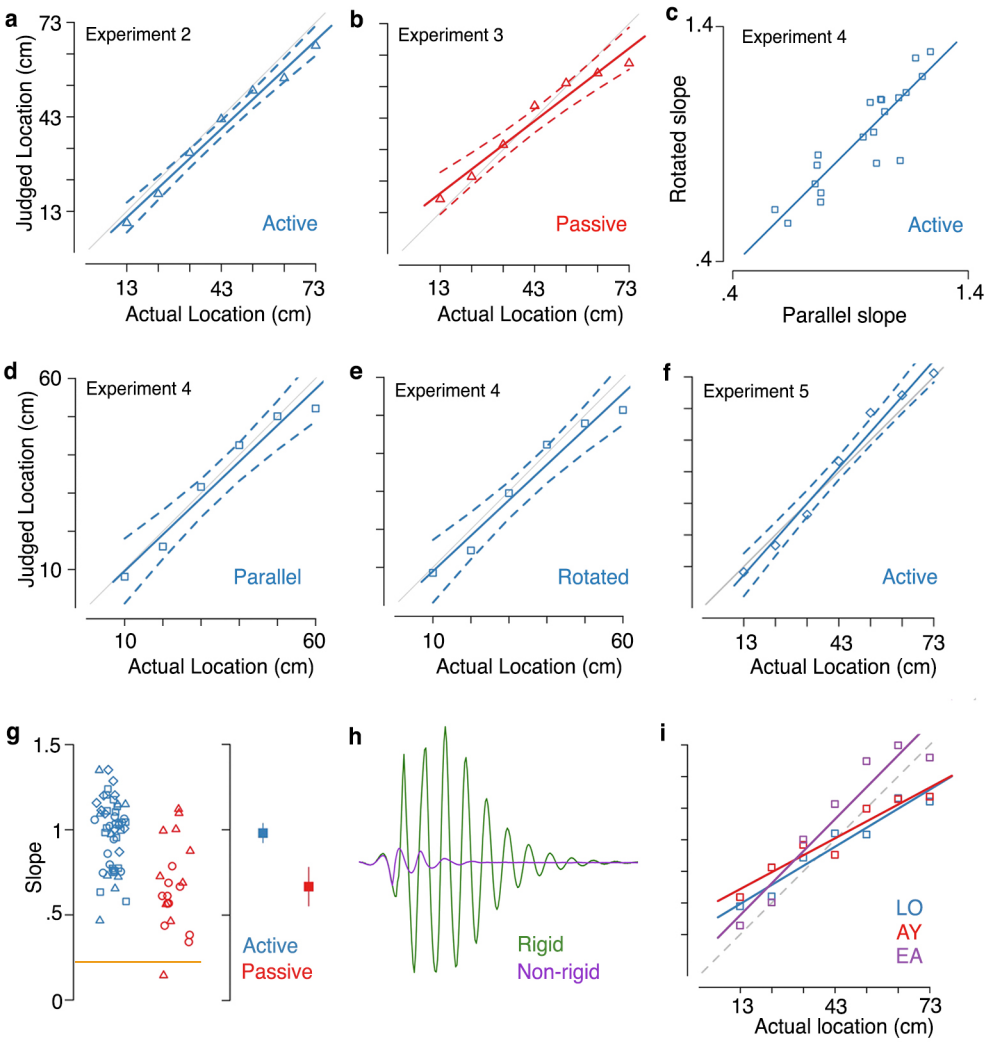

Extended Figure 2. Results of behavioural experiments
(a-f) Group-level affine regression for Experiment 2–5. Experiments 1, 2, 3, and 5 had an *n* of 10 and Experiment 4 had an *n* of 20. Coloured dashed lines around the model fits correspond to its 95% confidence interval. The grey line corresponds to the equality line. **(c)** Experiment 4: Pearson's correlation between the regression slopes for when the drawing was displayed in parallel with the actual rod and rotated 90-degrees counter-clockwise. **(g)** Left: Slope for every dataset from Experiments 1–5 (n=60). The distalisation model's prediction (i.e., chance performance) is shown by the orange line. Right: Average slope with 95% confidence intervals. **(h)** Experiment 6: Contact at identical locations on a wood (green) and foam (purple) tool leads to drastically different vibration patterns. In the case of the hybrid tool, participants could only feel the wooden portion of the rod with their hand, making the vibration pattern from the foam portion of the rod unexpected and therefore uninformative. **(i)** Localisation for each participant in the vibration experiment was within range of behaviour observed in the other six experiments.

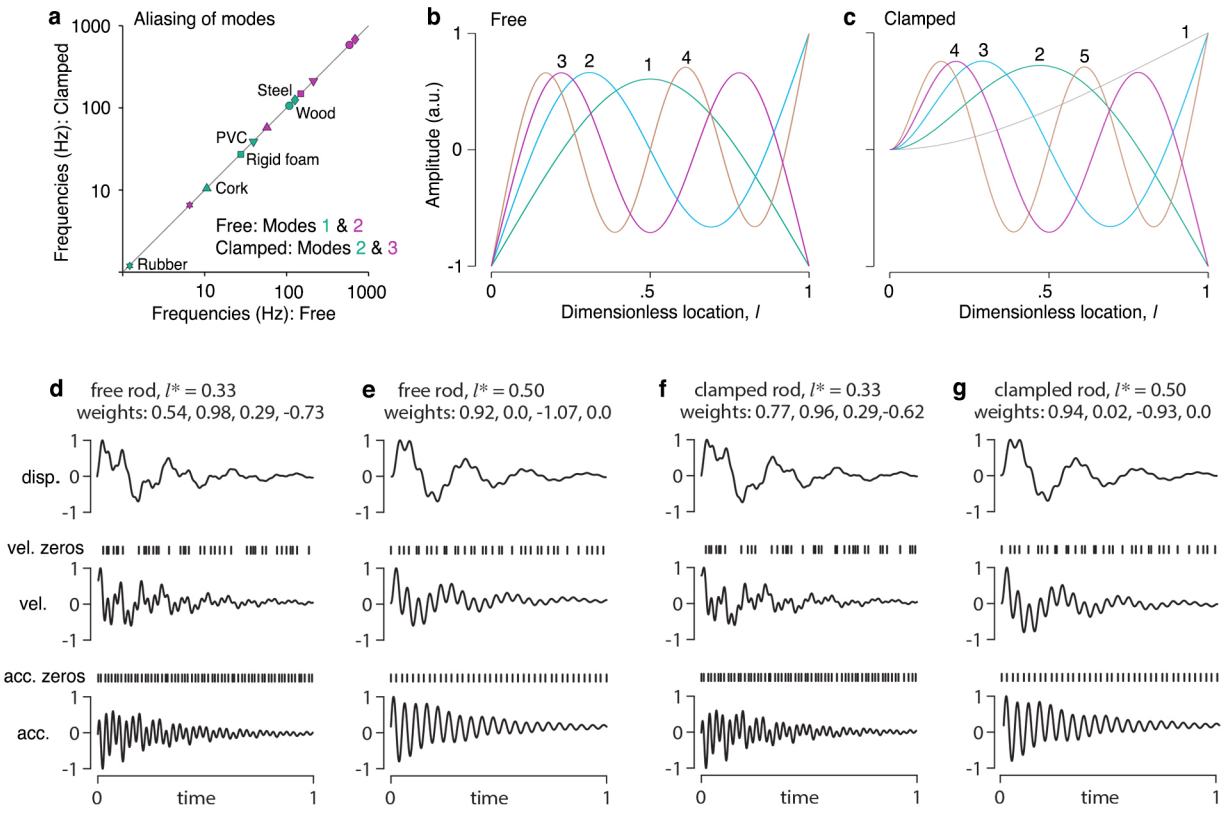

Extended Figure 3. Modal responses of a rod under different initial and boundary conditions
(a) Independent of the material of a rod, the modal frequencies in the free case alias to the next highest modes in the clamped case. In the plot, this can be clearly seen for a simulated rod with a circular cross-section (length: 83 cm; cross-section radius: 0.8 cm) that was made of one of a diverse set of materials of varying elasticities and densities. The grey line corresponds to the equality line between the frequencies of each limit case. **(b)** Mode shapes for the first four modes in the free case. **(c)** Modes shapes for the first five modes in the clamped case. Modes with similar shapes as the free case are matched by colour. **(d-e)** Simulated displacement, velocity, and acceleration following impact on a free rod at l^*=0.33 (**d**) and 0.5 (**e**). The zero crossings of velocity and acceleration are presented as tick marks above the relevant curves. The weights are taken from the mode shapes. **(f-g)** Same for the clamped case, but minus the 'whipping' first mode. This is justified since all other mode shapes and frequencies are shared between cases. Strikingly, there is a high degree of similarity between the modal responses in each case for impacts at identical locations. Furthermore, it can be noticed in all panels that the sequences of zero crossings tend to repeat themselves owing to the special distribution of modal frequencies reflected in the phase differences. After a few periods of the low frequency modes these sequences can generally be easily discriminated. Thus, an effective feature space could be simply a relatively small number of time intervals between extrema in a suitably filtered signal.

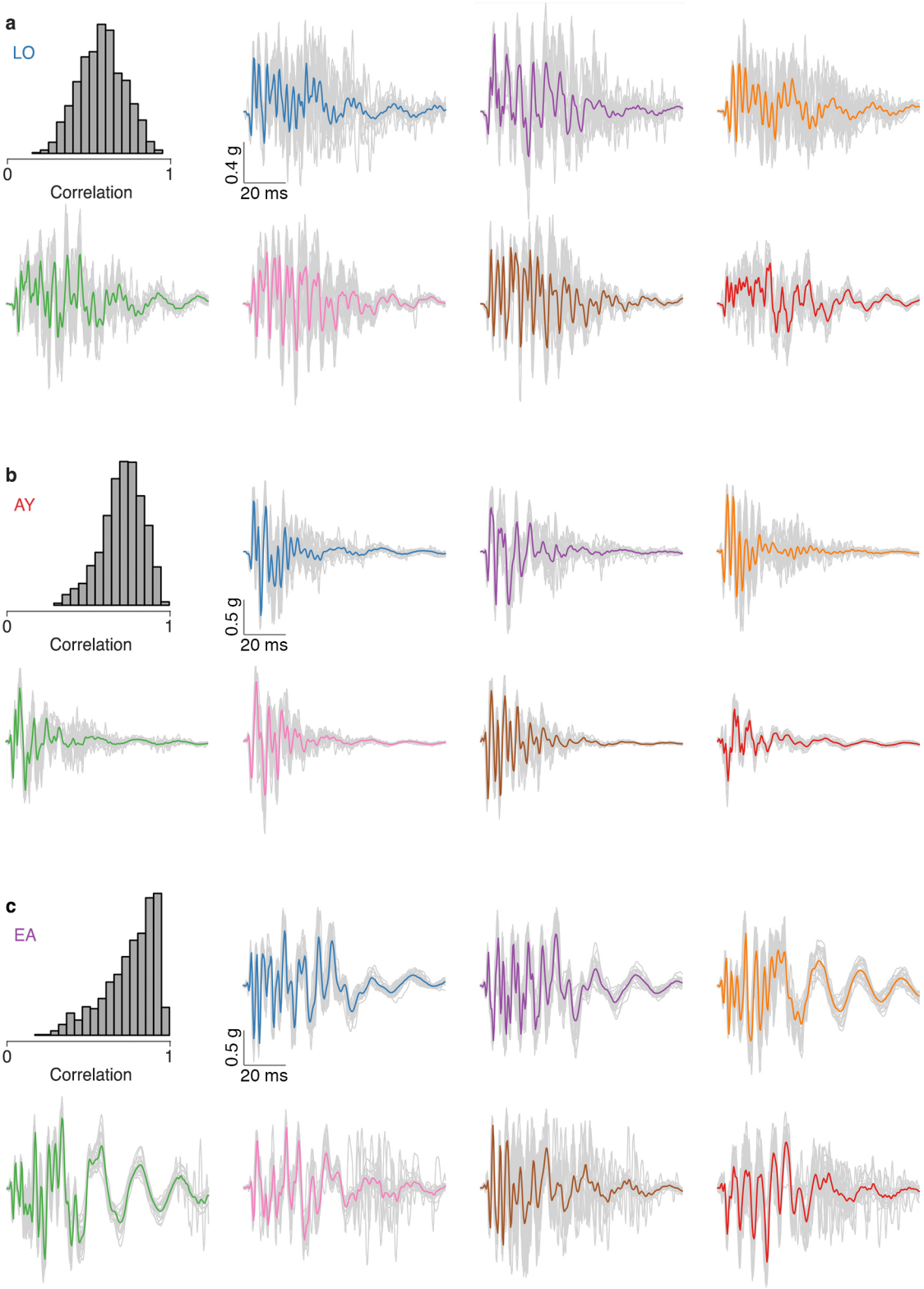

Extended Figure 4. Trial-by-trial vibrations for each participant were highly consistent
When held in the hand, vibrations following impact at each location on the tool were highly consistent for each participant: **(a)** LO, **(b)** AY, and **(c)** EA. The upper left plot in each panel corresponds to the histogram of each within-location Pearson's correlation (0–100 ms post-impact, corresponding to 250 data points per test). The shift in the distribution towards high correlations for each participant (LO: median r=0.58, IQR=0.19; AY: median r=0.73, IQR=0.16; EA: median r=0.79, IQR=0.23) provides

evidence for the emergence of vibratory motifs during passive and active sensing. The traces correspond to the motifs for each location (Landmark 1 [blue] to Landmark 7 [red], from left to right). The grey traces correspond to each individual impact and the colour traces correspond to the mean trace (0-100 ms post-impact; colour-coded by location).

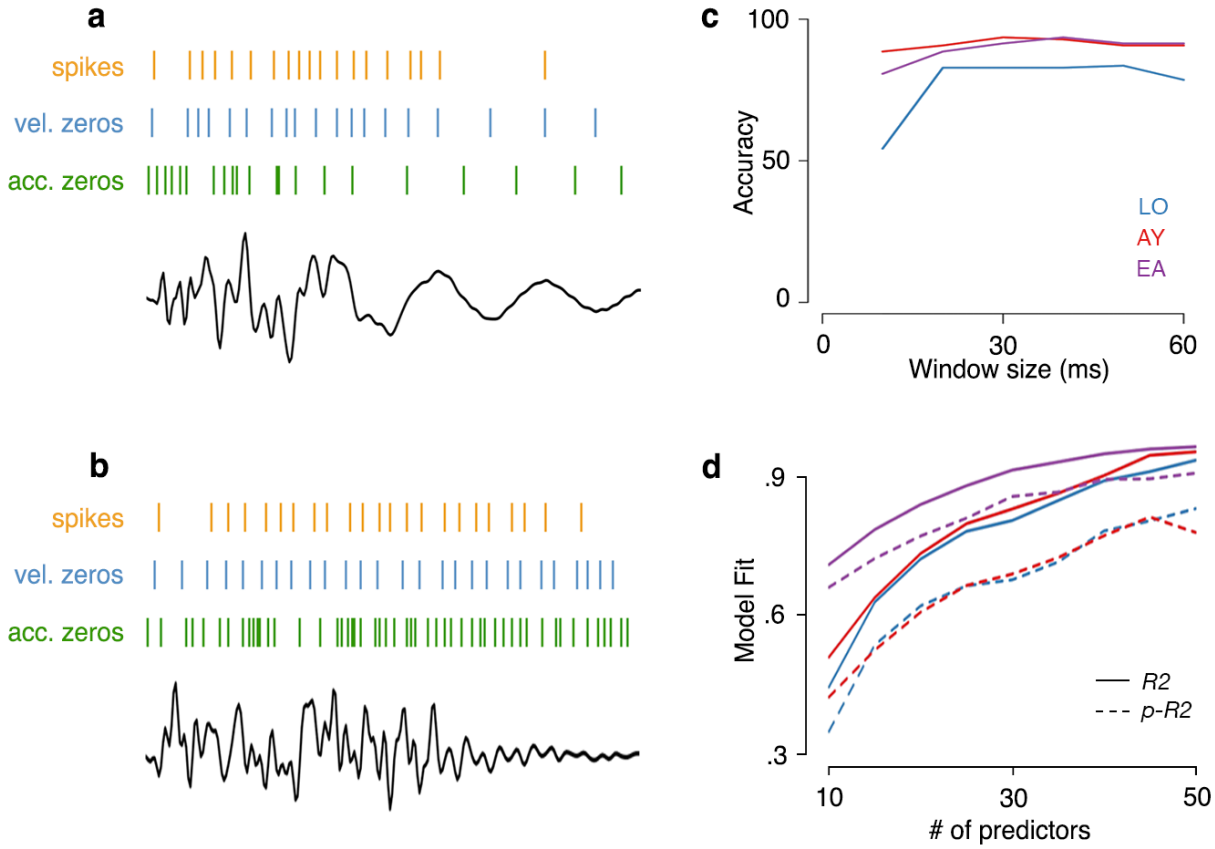

Extended Figure 5. The dimensionality of motifs can be reduced to their zero crossings
(a-b) The motif (black; acceleration), zero crossing in velocity (blue), and spikes (orange) of a representative trial from **(a)** EA and **(b)** LO's datasets. We observe a precise temporal relationship between zero crossings in velocity (blue) and the spikes of a Pacinian mechanoreceptor simulated with TouchSim (orange). **(c)** We observed high classification accuracy when decoding impact location from a motif's pattern of zero crossings in acceleration for each dataset (chance=~14%). **(d)** We could accurately model each participant's trial-by-trial behaviour given the temporal pattern of zero crossing in the corresponding motif's acceleration (140 data points per test). We plot the goodness of fit as a function of the number of predictors used in the model. Solid lines correspond to the R^2 and dashed lines correspond to the *predictive-*R^2.

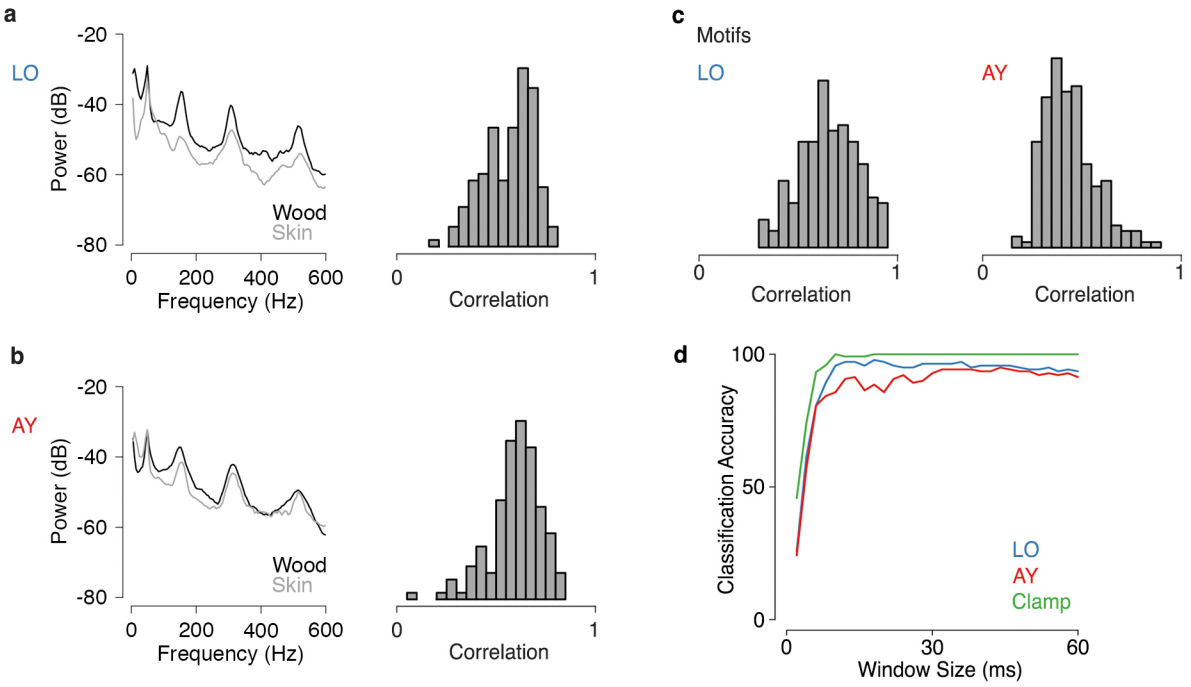

Extended Figure 6. Results for skin recordings

We found similar spectral content between the mechanical (tool) and cutaneous (D2m) vibrations for both **(a)** LO and **(b)** AY. Both participants showed similar peaks in the power spectrum for the vibrations (0–200 ms post-impact) on the tool (black line) and skin (grey line). Further, the trial-by-trial correlations between the spectral content of the wood and skin vibrations (histograms on the right) were high for both LO and AY. **(c)** Histograms of all within-location comparisons for participants LO (left; median r=0.65, IQR=0.21) and AY (right; median r=0.41, IQR=0.17); Pearson's correlation on the first 100 ms post-impact, corresponding to 250 data points per test. **(d)** The observed speed that location information accumulated within the vibrations on the skin was extremely rapid for each participant, mirroring what was observed when the tool was clamped with a bench vice (green line; see the experiment in the Supplementary Data Section 3).

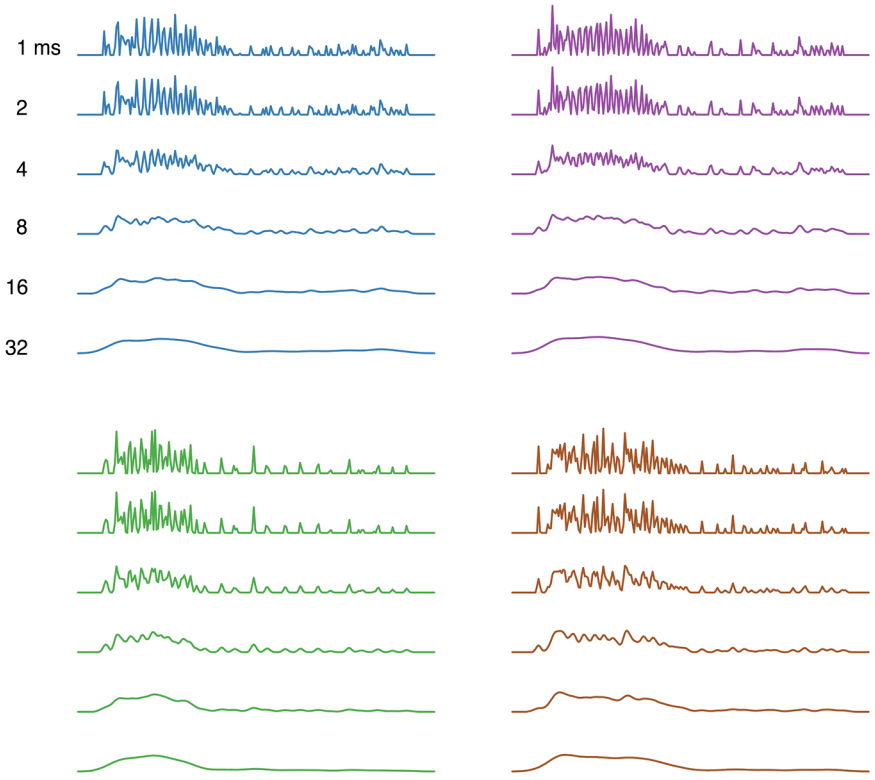

Extended Figure 7. The effect of temporal smoothing on population spiking
Population-level spiking (-15 to 215 ms post-impact) of the simulated afferents for randomly chosen trials from four different locations: Landmark 1 (blue; trial #12), Landmark 2 (purple; trial #39), Landmark 4 (green; trial #68), and Landmark 6 (brown; trial #114). To reduce the temporal resolution of spiking, we smoothed the response with Gaussian kernels at six different widths. The resulting traces were then used to investigate whether impact location coding was dependent on millisecond-resolution spike-timing (see Fig. 4d). Only trials from EA's dataset are shown in this figure, but nearly identical patterns of results were found for both LO and AY.

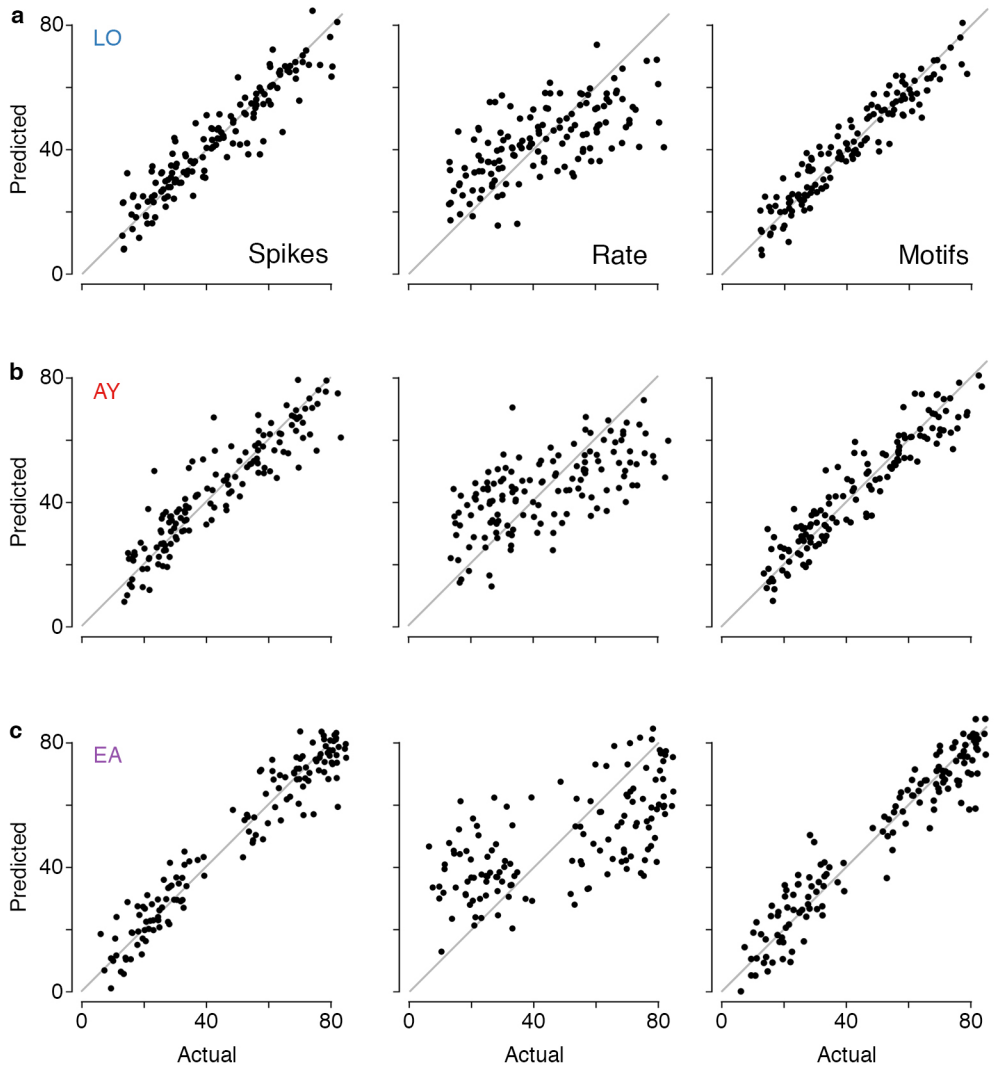

Extended Figure 8. Model fits for each participant.
The trial-by-trial population spike-timing of the putative afferents (left plots) precisely predicted the behaviour of each participant: **(a)** LO, **(b)** AY, and **(c)** EA. When the population rate code (centre plots) was used as features, the model did not provide a precise fit to the behaviour (see Data Table 1 and Extended Table 2). Vibratory motifs (right plots) also predicted behaviour with high precision. The grey line in all plots represents the equality line between actual and predicted behaviour, not the actual regression line.

Supplementary Data to **Sensing with tools extends somatosensory processing beyond the body** by L. E. Miller, L. Montroni, E. Koun, R. Salemme, V. Hayward, and A. Farnè

THE goal of our study was to investigate whether humans can sense the location of an impact on a tool. Six behavioural experiments provided strong evidence that humans are highly accurate at this task when using hand-held wooden rods. This striking result raises the question of the sensing mechanism that might be employed by the participants in the absence of a sheet of mechanoreceptors on a tool considered as a sensory extension of the body. We explored this question in the second part of the main text, leveraging ideas from structural mechanics and computational neuroscience. In essence, the participants solved an inverse problem. They mapped a rod's mechanical response to the location of an impact. These supplementary data are intended to clarify the underpinnings of this inverse problem and how the nervous system might solve it.

Inverse problems generally refer to the determination of the causes (e.g., impact location) from a set of observations (e.g., vibrations on the hand). Mathematically, inverse problems are posed in terms of a 'forward' model that predicts observations from parameters, and 'inverse' problems are solved when one finds the parameters from observations [39]. When the object under study is a dynamic system, such as a vibrating rod, inverse problems can take the form of the determination of the initial and/or boundary conditions of one or several differential equations.

We argued in the main text that the determination of the location of an impact on a hand-held rod given observed vibrations is akin to the determination of initial conditions, given an impulse response and a set of prior assumptions. It is important that the impact location be encoded in the vibratory signal in a manner that is largely invariant to such factors as the rod's material, its geometry, and the manner in which it is held. Here, we expand this proposal by going into greater theoretical detail than was possible there. The inverse problem considered here differs from problems typical in engineering where the source of excitation (i.e., the contacting object) is generally assumed to be known [40].

Section 1 of these Supplementary Data describes how contact location is encoded into the vibratory response of a rod. In Section 2 we develop a model of how contact location can be efficiently decoded by a process that could be supported by early stage neural computations. In Section 3, we describe the results of a pilot study that lent empirical support to these models.

1 Impact Location Encoding

1.1 The Euler-Bernouilli Beam

The vibrations of a straight, slender rod can be modelled by the solutions of a differential equation that is classically derived from the Euler-Lagrange minimisation principle of least action. This equation is found by considering the distribution of transverse kinetic energy and bending potential energy along a rod of length, L. If $x \in [0, L]$ designates the location along the rod and if only small deflections from the resting position, $u(x,t)$, are considered, this equation is the basis of the so-called the Euler-Bernouilli beam theory [41],

$$\underbrace{\frac{\partial^2}{\partial x^2}\left(E(x)I(x)\frac{\partial^2 u(x,t)}{\partial x^2}\right)}_{\text{from bending energy}} + \underbrace{\left(\mu(x)\frac{\partial^2 u(x,t)}{\partial t^2}\right)}_{\text{from kinetic energy}} = q(x,t). \tag{1}$$

The quantities $E(x)$ and $\mu(x)$ represent the mechanical properties of the rod. The quantity $E(x)$ is the elastic modulus of the material from which the rod is made. The elastic modulus captures the rod's material resistance to deformation. The quantity $\mu(x)$ is the rod's mass per unit of length, which depends on the rod's material and on its geometry. The quantity $I(x)$, called the second

moment of area, depends on the shape of the cross section. In general, these quantities depend on the location, x, along the rod. The quantity $q(x,t)$ presents the action of external objects at particular places on the rod and at particular times. It is hard to find the solutions of this equation in the general case.

However, if the rod is homogeneous and uniform (as was the case in Experiments 1-5) then E, I, and μ are constants. If, in addition, the rod is left free to oscillate, then the equation becomes an unforced ordinary differential equation. For ease of writing, the dependency of the displacement u on location and time can be implied in the foregoing and a damping term is added to model the fact that in most materials energy dissipates. Thus, (1) becomes,

$$EI\frac{\partial^4 u}{\partial x^4} + \mu\frac{\partial^2 u}{\partial t^2} + \lambda\frac{\partial u}{\partial t} = 0. \tag{2}$$

A differential equation that depends on time cannot be solved without the specification of initial conditions, that is of the state, $u(x,0)$, of the modelled object when $t = 0$. When it also depends on space, boundary conditions must specify how the state of the object and a sufficient number of derivatives should be treated at the boundary of the domain inside which the equation applies.

1.2 Canonical boundary conditions

Imagine a uniformly rigid rod that is clamped (i.e., held stationary) at one end and free to oscillate at the other. At the clamped end, the deflection is zero at $x = 0$, that is, $\forall t$, $u(0,t) = 0$, and the rod remains tangent to the clamp, $(\partial u/\partial x)(0,t) = 0$. At the free end, the rod does not bend since there is no moment applied, so the curvature and the change of curvature are zero, $(\partial^2 u/\partial x^2)(L,t) = 0$ and $(\partial^3 u/\partial x^3)(L,t) = 0$, which gives the four needed boundary conditions. A rod is said to be free when the free-end boundary conditions applies at $x = 0$ and at $x = L$, which also gives four boundary conditions.

A rod held in the hand can neither be modelled as perfectly clamped nor completely free. It would therefore be hazardous to attempt to model its effect using the aforementioned boundary conditions. The governing equation would need to be augmented with additional terms that take into the account the complex structural and mechanical properties of the hand's soft tissues, muscles, and bone structure. However, as highlighted in the foregoing, the solutions of (2) have similarities with boundary conditions as different as the clamped rod or the free rod. These cases may be viewed at the limit cases of a tight and a loose grip hand, giving boundary conditions that are "in between".

1.3 Modes

The solutions of (2) can be shown to have the form,

$$u(x,t) = \sum_{n=1}^{\infty} a_n(t) w_n(x). \tag{3}$$

Solutions thus decompose into an infinite sum of countable, discrete components. These components, called "modes", have the physical interpretation of the "standing waves" that give to physical systems in bounded domains, mechanical or otherwise, the propensity to oscillate at specific frequencies. In other words, the solutions of the unforced equation (2) exist only for certain frequencies called natural frequencies, ω_n, $n = 1, \ldots, \infty$. For small displacements, the modes are harmonic and thus their amplitudes have the form,

$$a_n(t) = A_n \sin(\omega_n t + \phi_n)\, e^{-\frac{1}{2}\frac{\lambda}{\mu}t}. \tag{4}$$

Modal solutions can in certain cases be truncated to a few terms, which is true for rods and other types of objects, such as strings and plates. Most slender rods tend to be underdamped, meaning that the modes do not decay too fast in time. We can take $\phi_n = 0, \forall n$ for the case of the unforced rod with an impulsive initial condition.

1.3.1 Modal Frequencies

The specific values of the natural frequencies depend on the geometry and on the material properties of the rod. If n is the mode number, the natural frequencies are,

$$\omega_n = \beta_n^2 \sqrt{\frac{EI}{\mu}}\,, \quad \text{where} \quad \beta_n = \eta_n \frac{\pi}{L}\,, \tag{5}$$

The η_n are constants close to unity or a few multiples of unity. They are specific to each boundary condition and inversely proportional to the rod length, L. The modal frequencies thus depend in the same way on the rod length so their ratios are *length-invariant*. The specific frequencies of each mode are predictable if and only if the geometry and the material of the rod are known, features that the human haptic system is specifically tuned towards detecting. It would be unsurprising if the nervous system was able to immediately predict the modal frequencies for a rod without prior experience wielding it. This prediction was indeed supported by the results of our fifth experiment.

The application of the boundary conditions of the free rod or of the clamped rod amounts to solving, $\cosh(\beta_n L)\cos(\beta_n L) = 1$ or -1, respectively, for the solutions to exist. The roots of these equations gives possible values for the β_n and hence for the η_n. For a free rod, the η_n are 1.5, 2.5, 3.5, 4.5, ...; for a clamped rod, they are 0.6, 1.49, 2.5, 3.5, 4.5, ... Clamping a rod rigidly at one end shifts the modal frequencies downward compared to a free rod. The influence of the boundary conditions is great in the low frequencies only (i.e., the lowest mode), but diminishes rapidly with increasing mode order.

We surmise that a human grip provides a boundary condition somewhere between these limit cases. Tightening a grip shifts the modal frequencies downward and promotes the occurrence of a low frequency "whipping mode" that does not exist in the free case. Mode 1 of the free case aliases to mode 2 of the clamped case, mode 2 to mode 3, and so on. Apart from the whipping mode, the natural frequencies, however, are indistinguishable between cases (Extended Fig. 3a). This is a critical point, because the grip strength of the tool user will likely change from moment-to-moment during tool-extended sensing. Thus, given that the frequencies of the higher modes are invariant to grip strength, the user will continually be "in tune" with the rod. As we will see in the next section, the encoding of impact location is also grip strength-invariant.

1.3.2 Mode Shapes

We now attend to the mode shapes, $w_n(t)$, in (3). It is these components that contains the impact location information. They have the form,

$$w_n = \underbrace{C_1 \cosh(\beta_n x) + C_2 \sinh(\beta_n x)}_{\text{non periodic part}} + \underbrace{C_3 \cos(\beta_n x) + C_4 \sin(\beta_n x)}_{\text{periodic part}}\,. \tag{6}$$

For the free rod and for the clamped rod, these mode shapes can be factored into simpler forms,

$$\text{free rod:} \quad w_n = C^{\text{free}} \left[(\sin\beta_n x + \sinh\beta_n x) - D_n^{\text{free}} (\cos\beta_n x + \cosh\beta_n x) \right]\,, \tag{7}$$

$$\text{clamped rod:} \quad w_n = C^{\text{clamp}} \left[(\cosh\beta_n x - \cos\beta_n x) + D_n^{\text{clamp}} (\sin\beta_n x - \sinh\beta_n x) \right]\,. \tag{8}$$

The factors C^{free} and C^{clamp} are scaling factors that can be taken to be equal to one since the initial amplitude of each mode depend solely on the initial conditions. The factors D_n^{free} and D_n^{clamp}, however, are functions of the boundary conditions. For the canonical cases at hand,

$$D_n^{\text{free}} = \frac{\sin\eta_n\pi - \sinh\eta_n\pi}{\cos\eta_n\pi - \cosh\eta_n\pi}, \quad \text{and} \quad D_n^{\text{clamp}} = \frac{\cos\eta_n\pi + \cosh\eta_n\pi}{\sin\eta_n\pi + \sinh\eta_n\pi}\,. \tag{9}$$

Calculations done, the D_n^{free} and the D_n^{clamp} turn out to all be close to one, except for D_1^{clamp} which is 0.734. We plot in Extended Figure 3b-c the dimensionless mode shapes, $\bar{w}_n(l)$, as a function of the dimensionless location $l = x/L$. As can be seen in these plots, like the modal frequencies, the shape of mode 1 of the free case is nearly identical to the shape of mode 2 of the clamped case, mode 2 to mode 3, and so on. Mode 1 of a clamped rod, the so-called 'whipping mode', does not have a counterpart in the vibrations of a free rod. Its natural frequency is low and is unlikely to be strongly excited in hand-held rod. It is therefore not taken into account in the analysis.

The mode shapes are notoriously sensitive to deviations from the assumptions of uniformity outlined in Section 1.1 , particularly as far as the mass distribution is concerned and less so from smooth variations of the cross section [41]. Mode shapes will be predictable to a tool user as long as the assumption of uniformity is not violated. This observation explains the results of the sixth experiment where, unbeknownst to the participants, we violated the uniformity assumption (see Methods and main text). The first half of the rod, the rigid portion, fulfilled the uniformity assumption and was usable as a sensor. The non-rigid portion, on the other hand, violated this assumption. Given that the predictable and unpredictable portions of the rod had very different modal responses (Extended Fig. 2h), it was impossible for users to sense impact location on the non-rigid portion.

1.4 Response to an Impact

The complex time domain response that we observe when we strike a rod arise from the peculiar distribution of modal frequencies that, unlike with strings, are not in integer multiples of a fundamental frequency. Like with strings, however, the different modes are selectively excited according the location of the excitation. For example, if an impact occurs at a location where the value of a mode shape is zero (see Extended Fig. 3b-c), called a 'node', this mode is not excited. If it is at an 'antinode' the excitation is maximum.

An impact is modelled by forcing an initial condition on velocity at one location, l^*. The condition, $(\partial u/\partial t)(l^*, 0) = v_0$, corresponds to the impulsive acceleration of an ideal inelastic collision at l^*. To model how the impact energy distributes among the different modes, consider that an impacted rod continues to vibrate subsequently to the impact where each mode oscillates with a decaying amplitude, initially of values A_n. From (4), the magnitude of the velocity of a particular mode at time 0 is $A_n\omega_n$. Thus, the total kinetic energy stored by mode n at time 0 is,

$$H_n(0) = \tfrac{1}{2}\mu L A_n^2 \omega_n^2 \int_0^1 \bar{w}_n^2(\zeta)\mathrm{d}\zeta \,. \tag{10}$$

The integral factor represents the contribution of a particular mode shape to the total vibration energy. Because these integrals evaluate to values close to one for all modes and for the two boundary conditions cases, the initial energy of a particular mode depends on its natural frequency and initial amplitude, but not on its shape. Call $\bar{H}_n(t)$ the energy of mode n of a rod of unit length and unit mass density, $\forall n$,

$$\bar{H}_n(0) \simeq \tfrac{1}{2} A_n^2 \omega_n^2, \quad \text{since} \quad H_n(0) \simeq \tfrac{1}{2} A_n^2 L \mu \omega_n^2 \,, \tag{11}$$

which is like the energy of a vibrating mass impulsed at time 0. The modal superposition (3) is truncated at some rank, although this step is not strictly necessary to keep the total energy finite. Touch being insensitive to frequencies higher than 1,000 Hz, we can select a truncation of rank, N, accordingly. An impact could well excite many higher modes, which could be heard, but only a few will drive the somatosensory system. Just after an impact at location, l^*, the total kinetic energy of a dimensionless rod is the sum of kinetic energy of each mode, $\bar{H}_n$, weighted by the square of the value of the mode shapes at that location,

$$\bar{H}(0) \simeq \sum_{n=1}^{N} \bar{w}_n^2(l^*)\bar{H}_n(0) = \tfrac{1}{2}\sum_{n=1}^{N} \bar{w}_n^2(l^*) A_n^2 \omega_n^2 \,. \tag{12}$$

Thus, we find that the modal amplitudes decay proportionally to the modal frequencies. Upon impact, each mode receives an initial velocity that is weighted by the value of the mode shape at the place of the impact and initial modal amplitudes are weighted the same way. The sign must be kept to preserve the total momentum.

1.5 Summary and Discussion

We can summarise the preceding discussion by the following observations.

1. Rods vibrate as a superposition of discrete modes, each of which is the product of a spatial component, called a mode shape, and a temporal component, which is a decaying harmonic oscillation at a natural frequency. The mode shapes and the natural frequencies depend on the boundary conditions.
2. The frequencies of each mode are not the multiples of a fundamental. For a given free rod, the frequencies are proportional to 1.5^2, 2.5^2, 3.5^2, 4.5^2, ... For the same rod clamped, the frequencies are proportional to 0.6^2, 1.49^2, 2.5^2, 3.5^2, 4.5^2, ... Clamping a rod adds a low frequency 'whipping' mode that is absent in the free case. However, the frequency of the first mode in the free case aliases the second mode in the clamped case, the second aliases the third, and so on (Extended Fig. 3a).
3. The influence of a hand grip on the modes can be thought of as somewhere in between the free and clamped cases. Given this, we can observe that a grip will 'tune' the modal frequencies of the first mode yet have little-to-no impact on higher modes.
4. The specific modal frequencies do however depend on how rods are made (Extended Fig. 3a), namely their material (i.e., elastic modulus and density), length, and cross-section shape, but not their ratios.
5. The amplitude of excitation of each mode depends on the relative location of a strike along the length of the rod (i.e., its mode shape). For equal initial excitations, the vibratory amplitude of each mode is inversely proportional to its frequency. Mode shapes have nodes where displacement is zero, which divide the length of the rod into coarse regions vibrating at different frequencies after an impact. The modes of the free rod are symmetrical about the centre, a symmetry that is broken for the clamped rod (Extended Fig. 3b-c).
6. When rods are underdamped, the spatial organisation of the vibrations is completely independent of how rods are made. Furthermore, mode shapes for a given condition (i.e., free or clamped) are invariant to grip strength, with the exception of the first mode. The shape of mode 1 of a free rod resembles mode 2 of a clamped rod, and so on.

Different conditions of mode excitation are shown in Extended Figure 3d-g to demonstrate the diversity of the temporal responses that can result from different boundary conditions and initial conditions. Extended Figure 3d and 3e shows the modal response of a free rod that has been contacted at l^* = 0.33 and 0.50, respectively. The plots show the vibration's displacement (upper panel) and its first two derivatives, velocity (middle panel) and acceleration (lower panel). Identical plots for the clamped case can be seen in Extended Figure 3f and 3g. Notice that in all cases the modal response is almost completely independent of whether the rod is free or clamped. Further, because differentiation emphasises the high frequencies, velocity and acceleration patterns (i.e., strain and strain rate) tend to be less influenced by the boundary condition than displacement patterns all the while preserving sensitivity on the location of impact (see results in the main text; Fig. 2). The tick marks above the plots of velocity and acceleration correspond to the point in time that they cross zero (i.e., zero crossing), a signal that could reduce the dimensionality of the motifs while preserving information about impact location (see Section 2).

The mode frequencies and shapes in the free case are aliased by the next highest mode in the clamped case (Extended Fig. 3a-c). The influence of grip strength on the modal response is somewhere in between these two limit cases. While grip strength will change over time during sensing,

this is unlikely to have a large influence on the velocity and acceleration of motifs. This point is underscored by our classification analysis (see main text) that combined the vibrations recorded from every participant, each of whom likely held the rod somewhat differently. Despite this, classification accuracy remained very high (Fig. 2e). Vibratory motifs therefore form a location-specific feature space (Fig. 2b) whose geometry is invariant across the material and structural properties of uniform rods and the boundary conditions set by the user's control policies.

Grip strength will, however, influences the decay rate of each mode. To explore grip behaviour during sensing, we recorded grip strength during the active and passive conditions. During active sensing, participants relaxed their grip when bringing the rod into contact with the object, a strategy that caused the vibrations to last longer. This is not a strategy used during passive sensing, because the participants could not anticipate when the impact occurred and therefore could not modulate their grip. This observation contributes to explain why location sensing was significantly more accurate during active sensing (Extended Fig. 2g).

2 Decoding the Location of Impact

2.1 Brief Recall of The Somatosensation of Vibrations

Having reviewed how impact location is encoded in the vibratory response of a rod, the question now is how it might be decoded by the nervous system. In vibrations, the displacement, the velocity, or the acceleration responses are different representations of the same signal. Whether they or any other derivative of the signal is used for analysis is a matter of convenience and of availability of appropriate sensors. In mammalian touch, certain sensor populations seem to be more sensitive to the strain and others to the strain rate of the tissues in which they are embedded [42, 43]. Selective sensitivity, however, depends on numerous factors, chief among them are the time scale of the evolution of strain and its magnitude, but sensitivity depends weakly on frequency. It would hazardous to assign a single sensor population to the task of providing the raw sensory input that enables observers to decode the impact location on a rod from its vibratory response.

Nevertheless, there exists a receptor population, known as Pacinian corpuscules, that is well suited for this task [44, 45]. Indeed, it is the location-specific responses of this population that we modelled using the TouchSim simulation package. In mammals the signals of different sensors are integrated as early as in second-order neurones and propagate through at least five neuronal layers before they can guide behaviour [46]. It is therefore worthwhile to consider the computational aspects of the decoding task from a broad perspective.

2.2 Computational Considerations

The primary aim of sensory information neural encoding is the reduction of tremendous dimensionality inherent to the raw physics of the world. A time-honoured signal processing approach that is favoured by engineers is frequency, and more recently, time-frequency analysis. The obvious advantage of these analyses is the dimensionality reduction they afford. A signal of infinite dimensionality can be reduced to a small number of components, provided that the signal has statistical properties that change slowly with time (or space), such as structural vibrations. While it is believed that the auditory system deploys a type of time-frequency analysis (i.e., 'gammatones') when processing sounds [47], a similar computational process does not seem to have any counterpart in the somatosensory system. Even if the somatosensory system can be coaxed into performing crude spectral discrimination, it seems ill-equipped to performing the fine decoding of impact location on a rod in the frequency or in the time-frequency domain, even if some measure of it could be called upon to enhance performance. Time domain analysis is a more suitable candidate and is more in line with known physiological, neuroanatomical, and behavioural data. It is for this reason that we focused on the time domain signals in our study.

2.3 Time Domain Decoding

In the time domain, the waveforms adopt different shapes as the order of differentiation increases since the high frequency modes become emphasised, see Extended Figure 3d-g. The simplest but perhaps the least computationally efficient approach taken by the nervous system would be to analyse the raw time domain signals. Such an approach ought not to be discarded completely since the mode shapes (Extended Fig. 3b-c) vary smoothly (in the mathematical sense of 'differentiability') with the location of impact. Thus, two impact locations which are neighbours on the rod also give rise of signals that are also neighbours in a feature space based on raw waveforms. Indeed, our experiment focused exclusively on accelerations signals in the time domain, demonstrating that they robustly encode impact location. While nothing in principle would preclude the realisation of such an approach by the nervous system, a computational process needed to extract impact location directly from the waveform has to contend with the infinite dimensionality of the raw signal space, although it is possible that the nervous system may use some criterion to discretise the signals. It is therefore enticing to consider more computationally efficient approaches to the decoding problem.

Other than by amplitude, information in a signal can be encoded by phase. The phase of an oscillatory signal is simply the argument of the sinusoidal functions that compose the complete signal. As per (4) there is one phase per mode considered, the $\omega_n t$, $n = 1, \cdots, N$. Thus, it is tempting to consider a feature space that is based on the phase differences between modes, since, like amplitudes, the phases differences encodes impact location. A naive approach to the computational process, then, would entail phase-accurate disentanglement of the different modes. The first step in such an analysis would resemble a short-term, phase sensitive spectral analysis, a process whose difficulty makes it unlikely to be implemented by the somatosensory system.

2.4 Extrema in Signals Encode Phase Interferences Between Modes

A more economical approach is to consider how the modes lead to the constructive and destructive interferences that determine the different waveforms. A well-known proxy for the occurrence of interferences in vibrations is the sequence of extrema in the signal. The somatosensory system might instead analyse the direct consequences of the *phase interferences* between modes. Here, the issue of selecting the appropriate derivative of the signal cannot be avoided. Given the known physiology of mechanoreceptors, it is reasonable to assume that the central nervous system receives information closely related to the occurrence of extrema of strain or of strain rate, which is equivalent to considering the zero-crossings of velocity and acceleration, respectively. Since the location-specific distribution of modal frequencies is reflected in the motif's phase differences (Extended Fig. 3d-g), analysing the timing of zero crossings would be a computationally efficient method for decoding impact location. This is reflected by phase-locking to the peaks of the next lowest derivative (i.e., displacement) (Extended Fig. 5a-b).

To assess the plausibility of this coding scheme, we re-analysed our data using the temporal patterns of zero crossings in the vibratory motifs. We found that the responses of the simulated Pacinian mechanoreceptors were almost perfectly phase-locked to the zero crossings of the velocity (i.e., peaks of displacement; Extended Fig. 5a-b). This remarkable result suggests that information-preserving dimensionality reduction occurs at the initial stages of somatosensory processing in the nervous system. We further found that (i) impact location could be accurately decoded from the temporal patterns of zero crossings of acceleration alone (Extended Fig. 5c); and (ii) that this pattern precisely predicted participant's trial-by-trial behaviour (Extended Fig. 5d). Thus, decoding impact location from the extrema in the time domain signal of a motif is not only a computationally efficient method of dimensionality reduction, but it is also physiologically plausible. Where and how this analysis is implemented in the nervous system [46] is a question the warrants future investigation.

3 Initial pilot study

As was discussed in Section 1, the time course of the displacements of all the points on the object is highly dependent upon the initial conditions, on the boundary conditions, and on the location of impact. As a pilot experiment to initially address the question of the informativeness of the vibratory response to impact, we probed the wooden rod's structural dynamics while it was clamped in place with a bench vice. The body of the rod was impacted at four evenly-spaced locations (13 to 43 cm) using a spring-loaded device. Vibrations were recorded (Analog Devices; Model ADXL335) from the handle (2.5 cm from the beginning of the handle) and the index finger (identical location) in separate datasets. Another accelerometer was attached to either the handle of the tool or the middle phalanx of the index finger from one of the authors (L.E.M.) as it pressed against the handle. For each surface, we recorded thirty trials per impact location (order randomized). All signal processing and data analyses were identical to those reported in the main article.

Multiple impacts at the same location producing consistent vibratory motifs both on the handle (median r=0.81, IQR=0.15) and on the index finger (median r=0.96, IQR=0.05). This result provided the initial hints for the existence of vibratory motifs. We then used support vector classification to characterise how location-specific information accumulated within these motifs over time (temporal window sizes: 2 to 100 ms, by steps of 2 ms). Classification accuracy for mechanical vibrations on the handle increased rapidly, reaching 90% accuracy within 28 ms (Fig. 2e). Remarkably, classification accuracy for cutaneous vibrations reached 90% almost five times faster (6 ms post-impact). It is interesting to note that this decoding speed is almost identical to what we observed in the experiment reported in the main article (see results and Fig. 2e), suggesting that the biomechanical properties of the hand actually enhance the location information encoded in motifs.

References

[39] Kabanikhin, S. I. (2008). Definitions and examples of inverse and ill-posed problems. *Journal of Inverse and Ill-Posed Problems*, 16(4):317–357.

[40] Barcilon, V. (1976). Inverse problem for a vibrating beam. *Zeitschrift für angewandte Mathematik und Physik ZAMP*, 27(3), 347–358.

[41] Coşkun, S. B., Atay, M. T., and Öztürk, B. (2011). Transverse vibration analysis of Euler-Bernoulli beams using analytical approximate techniques. In *Advances in Vibration Analysis Research.* InTech.

[42] Iggo, A., Ogawa, H. (1977). Correlative physiological and morphological studies of rapidly adapting mechanoreceptors in cat's glabrous skin. *Journal of Physiology* (London), 266:275–296.

[43] Johansson, R. S., Landström, U., Lundström, R. (1982). Responses of mechanoreceptive afferent units in the glabrous skin of the human hand to sinusoidal skin displacements. *Brain Research*, 244:17–25.

[44] Bell, J., Bolanowski, S. I. and Holmes, M. H. (1994). The structure and function of Pacinian corpuscles: A review. *Progress in Neurobiology*, 42:79–128.

[45] Saal, H. P., Wang, X., Bensmaia. S. J. (2016). Importance of spike timing in touch: an analogy with hearing? *Current Opinion in Neurobiology*, 40, 142–149.

[46] Bengtsson, F., Brasselet, R., Johansson, R. S., Arleo, A., and Jörntell, H. (2013). Integration of sensory quanta in cuneate nucleus neurons in vivo. PLoS One, 8(2), e56630.

[47] Smith, E. C. and Lewicki, M. S. (2005). Learning efficient auditory codes using spikes predicts cochlear filters. In *Advances in Neural Information Processing Systems*, pp. 1289-1296.